USGS
science for a changing world

Prepared in cooperation with the Connecticut Department of Energy and Environmental Protection

Characterization of Fractures and Flow Zones in a Contaminated Crystalline-Rock Aquifer in the Tylerville Section of Haddam, Connecticut

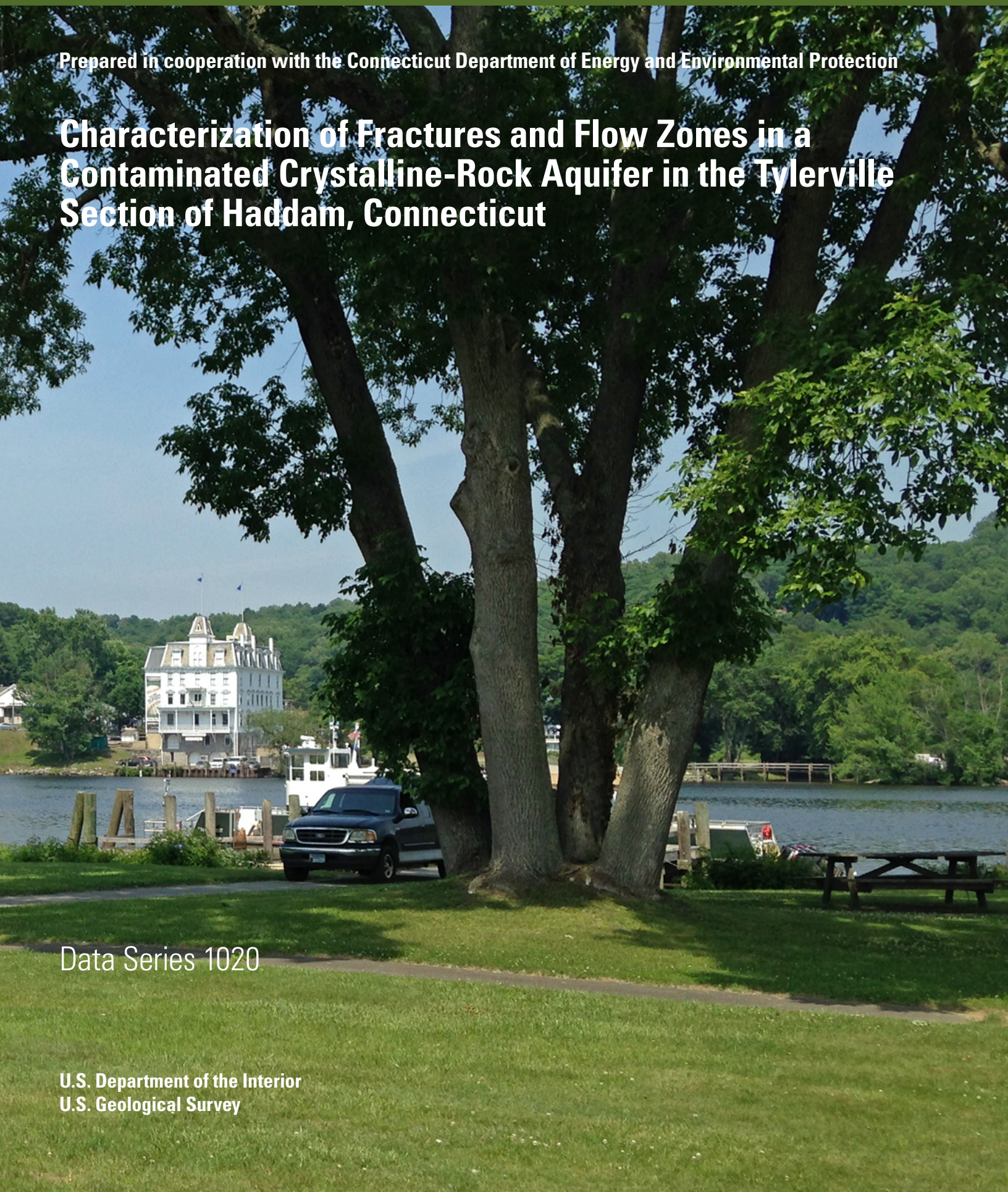

Data Series 1020

U.S. Department of the Interior
U.S. Geological Survey

Cover. View from Eagle Landing State Park in the Tylerville section of Haddam, Connecticut, shows the Swing Bridge over the Connecticut River with the Historic Goodspeed Opera House on the eastern shore in East Haddam, Connecticut.

Characterization of Fractures and Flow Zones in a Contaminated Crystalline-Rock Aquifer in the Tylerville Section of Haddam, Connecticut

By Carole D. Johnson, Kristal F. Kiel, Peter K. Joesten, and Katherine L. Pappas

Prepared in cooperation with the
Connecticut Department of Energy and Environmental Protection

Data Series 1020

U.S. Department of the Interior
U.S. Geological Survey

U.S. Department of the Interior
SALLY JEWELL, Secretary

U.S. Geological Survey
Suzette M. Kimball, Director

U.S. Geological Survey, Reston, Virginia: 2016

For more information on the USGS—the Federal source for science about the Earth, its natural and living resources, natural hazards, and the environment—visit http://www.usgs.gov or call 1–888–ASK–USGS.

For an overview of USGS information products, including maps, imagery, and publications, visit http://store.usgs.gov.

Suggested citation:
Johnson, C.D., Kiel, K.F., Joesten, P.K., and Pappas, K.L., 2016, Characterization of fractures and flow zones in a contaminated crystalline-rock aquifer in the Tylerville section of Haddam, Connecticut: U.S. Geological Survey Data Series 1020, 40 p., http://dx.doi.org/10.3133/ds1020.

ISSN 2327-638X (online)

Acknowledgments

This work was done in cooperation with the Connecticut Department of Energy and Environmental Protection. Shannon Pociu and Thomas RisCassi of the Connecticut Department of Energy and Environmental Protection, Bureau of Water Protection and Land Reuse, Remediation Division, contributed significantly to the planning and scope of this work. We appreciate the assistance of Karen Goldenberg and Gail Batchelder of Loureiro Engineering Associates and their staff including Jeremy Corcoran and Sean Buckley, who provided logistical assistance during the field effort. Additionally, the authors appreciate the homeowners who granted access to their wells for geophysical logging.

Contents

Figures

Tables

Conversion Factors

U.S. customary units to International System of Units

Multiply	By	To obtain
	Length	
inch (in.)	2.54	centimeter (cm)
foot (ft)	0.3048	meter (m)
	Flow rate	
foot per minute (ft/min)	0.3048	meter per minute (m/min)
gallon per minute (gal/min)	0.06309	liter per second (L/s)
	Specific capacity	
gallon per minute per foot [(gal/min)/ft)]	0.2070	liter per second per meter [(L/s)/m]
	Transmissivity	
foot squared per day (ft^2/d)	0.09290	meter squared per day (m^2/d)

Temperature in degrees Celsius (°C) may be converted to degrees Fahrenheit (°F) as follows:

$$°F = (1.8 \times °C) + 32.$$

Temperature in degrees Fahrenheit (°F) may be converted to degrees Celsius (°C) as follows:

$$°C = (°F - 32) / 1.8.$$

Datum

Vertical coordinate information is referenced to the North American Vertical Datum of 1988 (NAVD 88).

Horizontal coordinate information is referenced to North American Datum of 1983 (NAD 83).

Altitude, as used in this report, refers to distance above the vertical datum.

Supplemental Information

Transmissivity: The standard unit for transmissivity is cubic foot per day per square foot times foot of aquifer thickness [$(ft^3/d)/ft^2$]ft. In this report, the mathematically reduced form foot squared per day (ft^2/d) is used for convenience.

Specific conductance is given in microsiemens per centimeter at 25 degrees Celsius (µS/cm at 25 °C).

Bulk conductivity of the formation and fluids in the formation is given in millisiemens per meter (mS/m).

Measured pumping rates are given in gallons per minute (gal/min).

Sum of squared errors is given in gallons per minute squared $(gal/min)^2$ and expressed in E notation; that is, 3.0×10^{-14} is written as 3.0E-14.

In this report, the terms “borehole” and “well” are used interchangeably for convenience, with the understanding that borehole is a generic term for a drilled hole in the ground—including a well, which typically indicates a borehole completed for water supply.

Abbreviations

ATV	acoustic televiewer
bTOC	below top of casing
CT DEEP	Connecticut Department of Energy and Environmental Protection
E.	east (used for the reporting of fracture orientation)
EMI	electromagnetic induction
FEC	fluid electrical conductivity
FLASH	Flow Log Analysis of Single Holes
GUI	graphical user interface
HPFM	heat-pulse flowmeter
MHz	megahertz
MTBE	methyl *tert*-butyl ether
OTV	optical televiewer
PDF	portable document format
ROI	radius of influence
SC	specific conductance (at 25 degrees Celsius)
SSE	sum of squared errors
TEMP	temperature (log)
TN.	true north (used for the reporting of fracture orientation)
USGS	U.S. Geological Survey

Characterization of Fractures and Flow Zones in a Contaminated Crystalline-Rock Aquifer in the Tylerville Section of Haddam, Connecticut

By Carole D. Johnson, Kristal F. Kiel, Peter K. Joesten, and Katherine L. Pappas

Abstract

The U.S. Geological Survey, in cooperation with the Connecticut Department of Energy and Environmental Protection, investigated the characteristics of the bedrock aquifer in the Tylerville section of Haddam, Connecticut, from June to August 2014. As part of this investigation, geophysical logs were collected from six water-supply wells and were analyzed to (1) identify well construction, (2) determine the rock type and orientation of the foliation and layering of the rock, (3) characterize the depth and orientation of fractures, (4) evaluate fluid properties of the water in the well, and (5) determine the relative transmissivity and head of discrete fractures or fracture zones. The logs included the following: caliper, electromagnetic induction, gamma, acoustic and (or) optical televiewer, heat-pulse flowmeter under ambient and pumped conditions, hydraulic head data, fluid electrical conductivity and temperature under postpumping conditions, and borehole-radar reflection collected in single-hole mode. In a seventh borehole, a former water-supply well, only caliper, fluid electrical conductivty, and temperature logs were collected, because of a constriction in the borehole.

This report includes a description of the methods used to collect and process the borehole geophysical data, the description of the data collected in each of the wells, and a comparison of the results collected in all of the wells. The data are presented in plots of the borehole geophysical logs, tables, and figures. Collectively these data provide valuable characterizations that can be used to improve or inform site conceptual models of groundwater flow in the study area.

Introduction

From June to August 2014, the U.S. Geological Survey (USGS), in cooperation with the Connecticut Department of Energy and Environmental Protection (CT DEEP), collected a suite of borehole geophysical logs in six wells that have been monitored by the CT DEEP for contaminants, including chlorinated solvents and methyl *tert*-butyl ether (MTBE), and one former production well that had not previously been monitored by the CT DEEP (95–BR) (table 1).

The objectives of the study were to characterize the bedrock aquifer and identify the sources of water to selected boreholes in order to determine sampling locations within the boreholes and to refine the conceptual groundwater-flow model for the site. The CT DEEP selected the boreholes because contaminants had been detected in previous samples of tap-water produced from these boreholes or other nearby boreholes. To characterize the bedrock, borehole logging was conducted with methods including electromagnetic induction (EMI), gamma, caliper, fluid electrical conductivity, temperature, and optical and acoustic televiewer (OTV and ATV). Heat-pulse flowmeter (HPFM), borehole temperature, fluid conductivity, and fluid resistivity data were collected under ambient and pumping conditions to assess the overall borehole transmissivity as well as the discrete-zone transmissivity of major sources of water to the selected boreholes. Using single-hole flowmeter and water-level data, transmissivity and hydraulic head were determined for discrete fractures or fracture zones in each of the boreholes. For this investigation, detection was limited by the resolution of the HPFM, which is limited to fractures with a transmissivity greater than about 1E-5 feet squared per second; in addition, the dynamic resolution of the HPFM limits detection to fractures with transmissivity within one to two orders of magnitude of the most transmissive fracture in the borehole. Single-hole radar was used to characterize the location and orientation of fractures tens of feet from the borehole. Collectively these data can be used to improve the characterization of transmissive fractures that supply water to these boreholes and to refine the conceptual groundwater-flow model for the site. In addition, the hydraulic characterization of the fractures can be used to determine what points or intervals to sample within each borehole. Flow sampling techniques can exploit the well hydraulics such that grab samples can be positioned to sample water from inflowing fractures. The hydraulic data can also be used to determine what pumping rate is needed to reverse ambient flow.

Table 1. Wells investigated at the Tylerville study area, Haddam, Connecticut, 2014.

[Depths are below top of casing (TOC). Elevation of land surface data is provided by the Connecticut Department of Energy and Environmental Protection and has an accuracy of ±1 foot. Well locations are shown in figure 1. Time is given in 24-hour format. USGS, U.S. Geological Survey]

Well name	USGS well identification	Latitude, in decimal degrees	Longitude, in decimal degrees	Elevation of land surface, in feet	Land surface correction, in feet	Elevation of measuring point, in feet	Casing length, in feet	Total depth, in feet	Elevation of water level, in feet	Water level from TOC, in feet	Date and time of water-level measurement
1640–SR	CT–HD 476	41.4468	-72.47037	63	1.3	64.3	144.0	501.4	3.7	60.60	6/21/2014 10:30
85–BR	CT–HD 477	41.4489	-72.47182	70	0.0	70.0	141.2	230.0	7.5	62.50	7/30/2014 17:27
79/81–BR	CT–HD 478	41.44939	-72.47217	73	0.5	73.5	138.0	230.0	7.0	66.50	8/5/2014 11:54
76–BR	CT–HD 479	41.45038	-72.47234	76	1.0	77.0	151.0	301.0	-12.0	89.00	7/29/2014 11:30
77–LMR	CT–HD 480	41.44668	-72.46486	7	0.8	7.8	155.5	343.8	2.3	5.47	6/26/2014 10:30
130–LMR	CT–HD 481	41.44316	-72.46452	4	2.3	6.3	108.5	345.0	-.35	6.65	6/24/2014 18:10
95–BR	CT–HD 482	41.44824	-72.472155	70	0.0	70	146?	308.0	3.61	66.39	8/1/2014 12:05

Description of the Study Area

The study area is in the village of Tylerville, in the southern part of Haddam, Connecticut, on the western bank of the Connecticut River. The study area is along Bridge Road (Route 82), east of Route 154, and west of the Connecticut River (fig. 1). The land surface slopes generally from the west to the east and from north to south. There is a well-defined ravine that has seasonal flow toward the Connecticut River. Land use in Tylerville is mixed and includes residential, light industrial, and commercial areas.

Previous Investigations

Site investigations and characterizations of contamination have been conducted over the last three decades. Since the 1980s, as many as 19 domestic wells in the study area have been contaminated above health-based drinking water standards with chlorinated volatile organic compounds, including trichloroethylene (TCE) and its decay products. More recently, in the mid-2000s, 1,4-dioxane was identified as a co-contaminant in several of the polluted wells (Connecticut Department of Energy and Environmental Protection, 2015). In addition, five other wells on commercial properties have been contaminated with MTBE, which was used as a gasoline additive. In order to identify possible sources of the groundwater contamination affecting potable wells in Tylerville, the CT DEEP commissioned a "Modified Phase I Environmental Site Assessment and Review of Historical Data Report for Tylerville Center" (AECOM, 2010). The CT DEEP was engaged in enforcement actions at two sites in Tylerville in 2013 and is currently (2016) undertaking a regional hydrogeologic investigation. This work involves determination of sources of contamination and characterization of the contaminant distribution. As part of these investigations, the CT DEEP wants to improve characterization of the bedrock, the fracture system, and the conceptual model of groundwater flow and contaminant transport for the site.

Photo lineament mapping and bedrock field outcrop mapping of fractures and foliation were conducted by the CT DEEP Site Assessment and Support Unit. In that investigation, 73 photo lineaments were identified. Although the longest features had a trend of true north (TN) TN. 150° to 180° E., the majority of features had a trend of TN. 45° to 90° E. (James Fitting, written commun., CT DEEP Memorandum "Lineament and Fracture Mapping," August 29, 2013, revised on January 27, 2016).

Fracture characterization of local bedrock outcrops was summarized by the CT DEEP (James Fitting, written commun., CT DEEP Memorandum "Lineament and Fracture Mapping," August 29, 2013, revised to January 27, 2016). A total of 42 fractures were identified on 13 outcrops in a study area that was west of Route 154 and the current borehole geophysical investigation. Fifteen of the fractures were clustered in two populations—one with an average strike of TN. 50° E. and the other with an average strike of TN. 240° E., with steep dips of 70 to 90° to the southeast and northwest, respectively. Nine fractures had an average strike of TN. 71° E., dipping 78° to the southeast. Foliation (based on five observations) is identified on these outcrops and is fairly flat-lying, with an average strike of TN. 60° to 90° E. and a dip of 23° to the southeast.

In another fracture study, fractures were observed in four outcrops to the west of Route 154 by Loureiro Engineering Associates, Inc., in December 2013 (Gail L. Batchelder, written commun., Letter to CT DEEP, June 11, 2014). They noted that no bedrock outcrops have been located within the study area, and the only exposures are located to the west of Route 154. Their investigation supplemented the fracture characterization summarized in the August 29, 2013, CT DEEP memorandum. The fractures in the supplemental fracture investigation had three dominant strikes: TN. 60° to 75° E., TN. 90° to 120° E., and TN. 165° to 180° E., with dips to the east-southeast, south-southwest, and west-northwest, respectively. About two-thirds of the mapped fractures are steeply dipping, and the other third are shallow and similar to the foliation of the bedrock. Foliation in these outcrops has strikes of TN. 108° E. and TN. 198° E., with shallow dips (2 to 18.5°) at low elevations on the outcrops and steeper dips (26 to 30°) at high elevations on the outcrops. In general, the foliation dips at shallow angles to the south and west.

Geologic Setting

At the 1:125,000 scale of the Connecticut State geologic map, the bedrock in the study area consists of Silurian quartz-biotite schist and calc-silicate gneiss (Rodgers, 1985). Geologic mapping of the Deep River quadrangle, which includes Tylerville, identified multiple metamorphic rock units (Lundgren, 1963), including the Hebron Gneiss, an interbedded quartz-biotite schist and fine-grained, equigranular, calc-silicate gneiss, which includes a dark-greenish to gray diopside calcium-magnesium amphibole. The USGS (2015) describes the Hebron Gneiss as follows:

> Silurian to Ordovician in age: Interlayered dark-gray, medium- to coarse-grained schist, composed of andesine, quartz, biotite, and local K-feldspar, and greenish-gray, fine- to medium-grained calc-silicate rock, composed of labradorite, quartz, biotite, actinolite, hornblende, and diopside, and locally scapolite. Local lenses of graphitic two-mica schist.

Although large-scale faults have been mapped to the south and west of the study area (Rodgers, 1985), none have been mapped in the study area. However, there is a large network of fractures in the crystalline rock that constitutes the bedrock aquifer in the study area. Water is typically stored and transmitted through joints, fractures, and faults in crystalline rock in a network of secondary porosity; the primary porosity in crystalline rock is negligible, but can be important for contaminant storage (Parker, 2007).

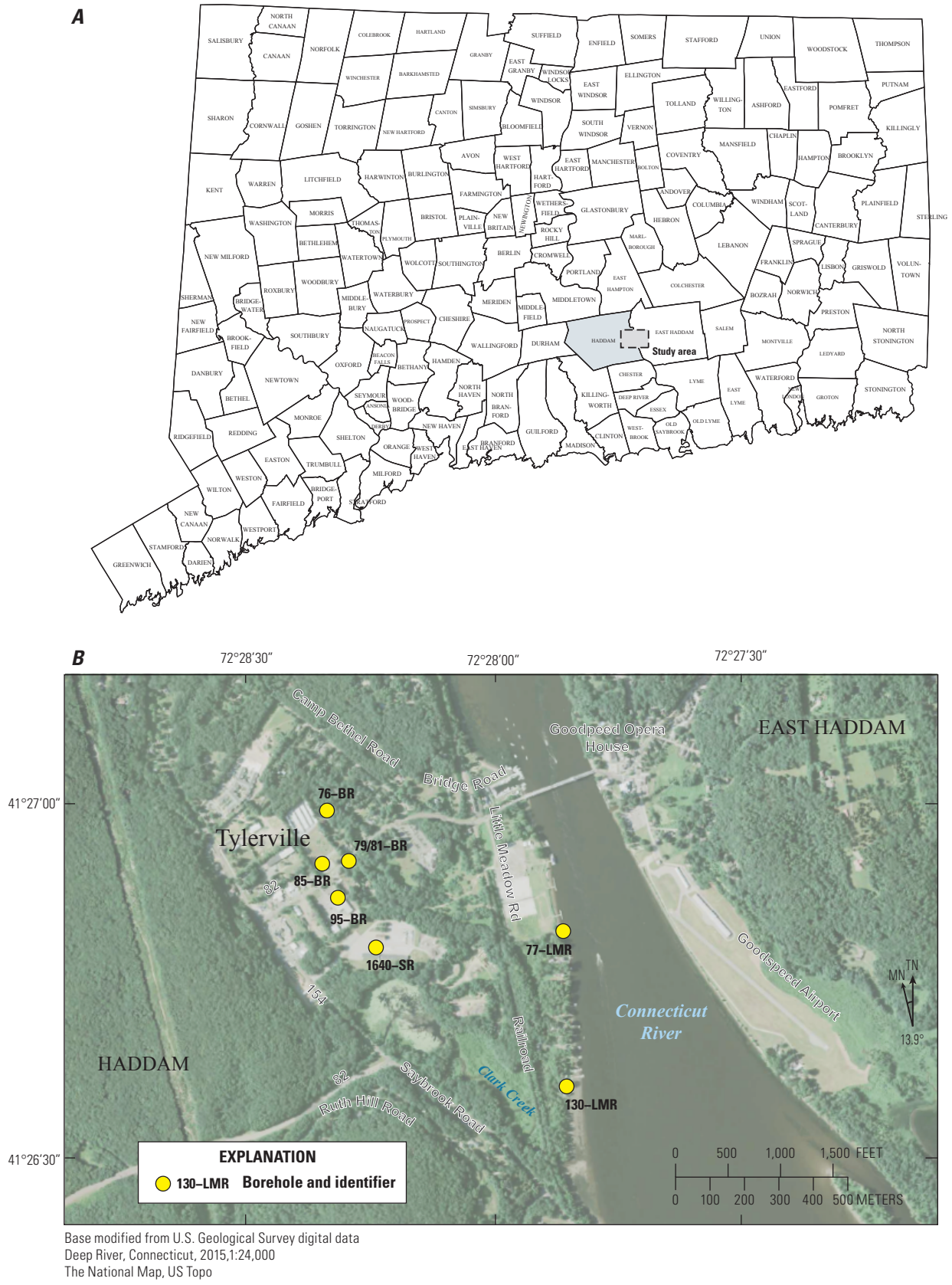

Base modified from U.S. Geological Survey digital data
Deep River, Connecticut, 2015,1:24,000
The National Map, US Topo

Figure 1. *A*, Map of Connecticut towns and study area and *B*, map showing location of boreholes in the study area in the Tylerville section of Haddam, Middlesex County, Connecticut. MN, magnetic north; TN, true north.

The unconsolidated deposits in Tylerville consist of alluvium, stratified drift, ice contact, and lacustrine deposits, and vary from fine to coarse sand with some gravel, traces of silt and clay, and a thin veneer of till. Detailed stratigraphic logs from two overburden wells show that the unconsolidated deposits extend to 138 feet (ft) below land surface (Handman and Bingham, 1980). Stone and others (2005) describe the overburden units as lower Connecticut River deltaic deposits, alluvium, and saltwater- or freshwater-marsh deposits.

The depth to rock in the study area has been mapped by using various geophysical methods as part of the ongoing CT DEEP investigations. A total of 176 passive seismic measurements were collected by the USGS in Tylerville in 2014 by using the horizontal-to-vertical spectral ratio (HVSR) method. This technique can be effective for identifying the depth to rock where there is a strong contrast in the acoustic properties of the overburden and the bedrock (Lane and others, 2008; Fairchild and others, 2013). The results indicate that depth to rock varies from 0 (along the valley wall) to 200 ft (Johnson and Lane, 2016).

Purpose and Scope

This report summarizes the purpose, methods of investigation, data processing, and results of borehole geophysical investigations conducted in July and August 2014 in Tylerville, Conn. The report includes descriptions of borehole geophysical and hydraulic data collected from six domestic wells and one former production well completed in bedrock. Mechanical caliper logs, borehole imaging, EMI conductivity, and deviation logs were used to confirm borehole construction and borehole integrity. Borehole logging methods, including gamma and EMI conductivity, were used to determine changes in the geologic formations that might indicate contacts of rock types. Borehole imaging, including ATV and OTV, was used to identify the location and orientation of bedrock fractures. Borehole radar, including directional and nondirectional methods, imaged reflectors in the formation around the borehole. Fluid and hydraulic properties of the aquifer were determined by using the fluid logging tool, which measures the fluid electrical conductivity (FEC) and the temperature (TEMP). The HPFM was used to measure vertical flow in the borehole and to determine the depth of inflow and outflow under pumping and ambient conditions. The results are described for each of the wells in the section "Data and Results by Well." The data are presented in figures, tables, and plots in the appendixes to the report.

Methods of Investigation

The geophysical logs were collected from June to August, 2014. Multiple borehole-geophysical logs were collected to characterize the well construction, rock properties, fracture pattern, and hydraulic properties in six boreholes at the study area. Logging of borehole 95–BR could not be completed because of obstructions encountered in the borehole that prevented deployment of all geophysical tools. In addition, water-level data were collected during pumping to estimate the open-hole transmissivity and natural groundwater fluctuations. All depths given are from below top of casing (bTOC).

Data Collection

Caliper, EMI, OTV, and ATV logs were used to verify the well construction, including casing diameter and length, casing material, total depth, and presence of foreign objects. EMI, natural gamma, and OTV logs were used to characterize the rock units. In addition, caliper, ATV, OTV, and nondirectional and directional borehole-radar logs were used to characterize fractures. FEC, TEMP, and specific conductance (SC) logs were used to characterize the hydraulics and general water quality. All data were combined, and preliminary field interpretations were used to guide the collection of subsequent logs—specifically the flowmeter data. HPFM logging of the wells was done under ambient and pumping conditions. In the six boreholes where the complete suite of borehole logs was collected, the logs were generally collected in the order of the following list.

- FEC and TEMP logs were collected first in the undisturbed water column. Under ambient flow conditions, these logs are valuable for identifying inflow and outflow zones. Changes in the measured parameters can indicate hydraulically active fractures. Departures in temperature from the geothermal gradient, which is approximately +1° per 100 ft of increased depth, can help identify hydraulically active zones. Straight-line segments with the same water temperature and (or) fluid conductivity can indicate vertical flow in the borehole. By differencing the logs collected under ambient and stressed (pumping) conditions, inflow zones that contribute to the well under pumping conditions can be identified. The inflow of these fractures can be less than the resolution of the flowmeter tools. This differencing of FEC and TEMP can be effective for identifying inflow zones that might not be identified with flowmeter tools alone.

- Caliper, which is typically collected as the second log, was used to assess the overall integrity of the borehole and verify the construction—including depth, casing diameter, and borehole enlargements—and possible constrictions. The caliper logs, along with imaging logs, were used to optimize placement of the flowmeter during logging and to assess the quality of the vertical flowmeter measurement.

- OTV and ATV logs were critical for mapping the locations and orientations of fractures and rock types in the boreholes. Optical image data were collected by going down the well to minimize the disturbance of

the water and avoid turbidity. When possible, the OTV was used as the first log on the second day of logging, after a night of allowing the water to settle. The OTV and ATV helped differentiate changes in rock type and lithologic features from structural features such as fractures. The fracture location, borehole diameter, and borehole rugosity (or roughness of the borehole wall) were used to optimize the placement of the flowmeter.

- Deviation log data were collected as part of the OTV and ATV logs. A three-component flux-gate magnetometer was used to measure the x-, y-, z-position of the borehole. Deviation data were used to correct the orientations of features observed in the image logs. EMI logs were collected to help determine the depth to the bottom of casing, identify changes in lithology, and guide the interpretation of borehole-radar data. EMI logs provide a measurement of the bulk conductivity of the formation and fluids surrounding the borehole. Measurements are in millisiemens per meter (mS/m) with a vertical resolution of about 2 ft. The measurement is relatively insensitive to the conductivity of the fluids in the borehole for diameters less than about 8 inches.

- Natural gamma logs were used to identify changes in lithology. Gamma logging measures the naturally occurring gamma radioactivity of the formation surrounding the borehole. The most common sources of gamma activity are potassium 40, which is abundant in feldspar and mica, and daughter products of uranium and thorium decay. The vertical resolution of the gamma probe is about 1 ft, and it can sense radiation through polyvinyl chloride (PVC) and steel casing.

- HPFM logs collected under ambient and stressed (pumping) conditions were used along with hydraulic head data to identify and characterize the transmissivity and head of individual fractures in the boreholes. Measurements were collected at stationary locations above and below fractures. With the limitations of resolution and dynamic range of the HPFM, typically two to four fractures are identified per borehole. Additional details on HPFM logging, processing, and interpretation are provided in the Heat-Pulse Flowmeter and Quantitative Analysis of HPFM.

- Directional and nondirectional single-hole surveys of radar reflectors were conducted in each borehole to identify the location and orientation (if possible) of reflectors and the projected intersection to the borehole—below the drilled depth of the well, behind the casing, or above the land surface. Reflectors projected to above the land surface are indicated with a negative depth. In addition, each reflector was described in terms of its spatial continuity and its relative reflection strength. The radial depth of penetration is estimated by examination of the radar logs. Where fracturing is intense, individual reflectors and fractures might not be uniquely identified, but zones of fractures can be identified in the radar records. Additional details on radar logging, processing, and interpretation are in the "Borehole Radar" section.

For a more general description of the methods used in this investigation, see Keys (1990). All data were collected in accordance with American Society for Testing and Materials (ASTM) guidelines where available. Specifically, D6167–97 (2004) and D6726–01 (2001) were used for mechanical caliper and EMI logging, respectively. Practical applications of these tools for the characterization of fractured rock, with information on techniques of calibration and quality assurance, is provided by Johnson and others (2011).

Borehole Radar

Radar is distinctly different from the other borehole logs. The radar tools image the formation surrounding the borehole, whereas the other logs sample the formation and fractures in the borehole or immediately adjacent to the borehole. In resistive rock units, radar can image the formation tens of feet from the borehole. Borehole-radar reflection logging uses a pair of downhole transmitting and receiving antennas to record the reflected wave amplitude and transit time of high-frequency electromagnetic waves (fig. 2*A*). For this investigation, 60- and 250-megahertz (MHz) antennas were used. The electromagnetic waves emitted by the transmitter penetrate into the formation surrounding the borehole and are reflected off a material with different electromagnetic properties, such as a fracture or a change in rock type (figs. 2*A* and *B*). Radar methods are described in detail by Lane and others (1994), and a practical application is provided by Johnson and Joesten (2005).

The velocities of the radar waves in the bedrock surrounding the boreholes were determined by using single-hole vertical radar profiling with the 250-MHz antennas. The velocities were determined for each borehole by using methods described by Buursink and others (2002). For this investigation the velocities ranged from 384.5 to 396.7 feet per microsecond (ft/µs). These velocities were used in the determination of the dip of reflectors identified with the 60-MHz directional radar data. The resistive rock units appear to be ideal for radar wave propagation, as there was little attenuation caused by conductive rock units.

The nondirectional data were imported into WellCAD, a borehole log display and interpretation program (http://www.alt.lu). These data were analyzed for direct arrival time (fig. 2*B*). Picking the traveltime was automated by using a full-waveform sonic package in WellCAD. The automated picks were adjusted manually when necessary. The velocity was computed by using the transmitter-receiver separation distance divided by the traveltime of the direct arrival. The dielectric permittivity was computed by using the relation

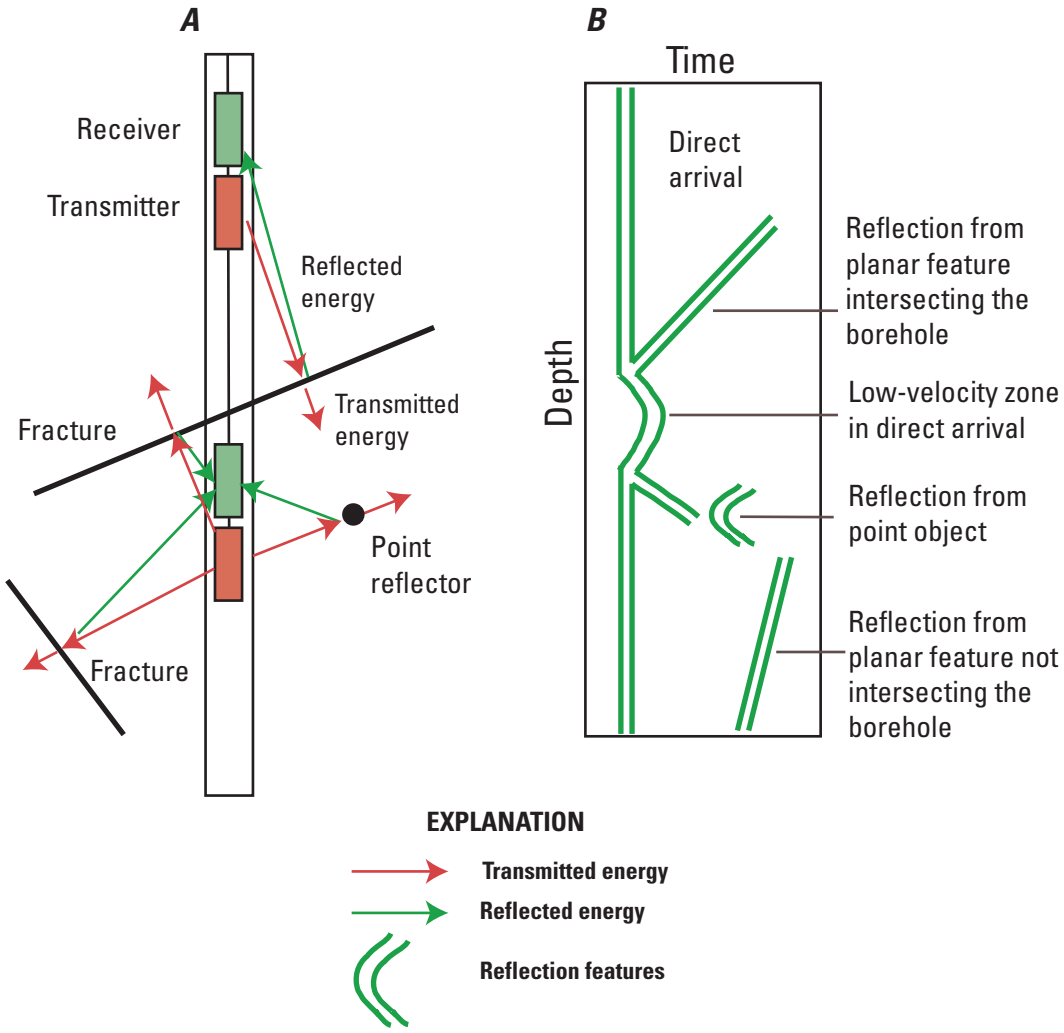

Figure 2. Borehole-radar schematics showing *A*, transmitter and receiver configuration in single-hole reflection and *B*, typical reflection patterns for direct arrival, point reflectors, planar reflectors that intersect the borehole, and reflectors whose projections intersect the borehole below the drilled depth or above the land surface. Figure modified from Lane and others (2001, fig. 2).

of the square of the ratio of the speed of radar in air divided by the measured velocity. Thus the dielectric permittivity is inversely proportional to the velocity through the material. In addition, the amplitudes at the first positive and first negative arrival peaks were extracted, and the peak-to-peak amplitude (in microvolts) was computed in WellCAD. The attenuation, which is a measure of the signal loss in the formation, was estimated by using the peak-to-peak amplitude normalized by the outgoing amplitude for the antenna per unit length. Attenuation is usually shown in decibels per unit length (a logarithmic expression for power loss over length). In this application, the loss of signal can be related to conductive boundaries, water-filled fractures relative to the solid rock, and discontinuities in the rock. Thus the combination of decreased velocity and increased attenuation is consistent with water-filled fractures. Velocity, dielectric permittivity, and attenuation logs provide unambiguous indicators of water-filled fractures. These datasets are provided in the appendixes.

Determination of planar reflectors and orientation was done in the RAMAC processing software. After the data were filtered and processed, planar features were manually fit to the radar reflectors observed in the radargrams (fig. 3*A*). The directional antenna resolves the radar response from 36 discrete planes in 10-degree increments surrounding the boreholes (figs. 3*B* and *C*). Each reflection in the radargram is analyzed separately. The determination of strike of reflectors is described in detail in Johnson and Joesten (2005). Each plane was examined for reflectors, and planar features were fit to the reflector in the interactive software. In the best situation, both limbs are clearly viewed and an interpretation of structure can

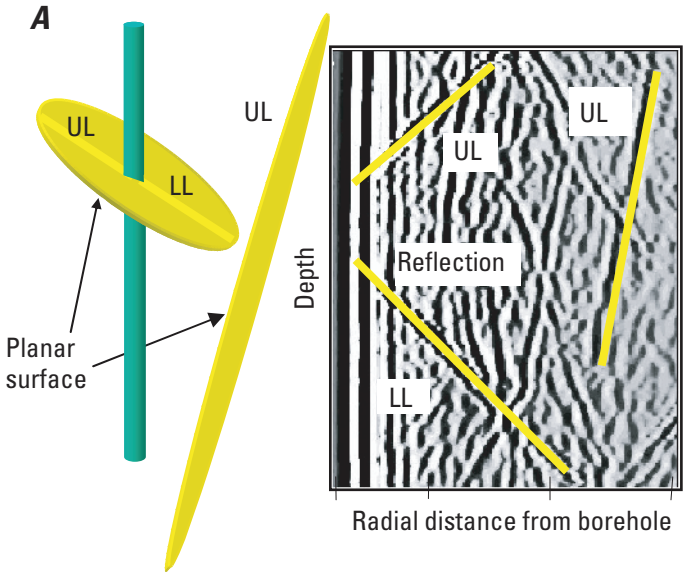

A radargram, or radar-reflection profile, shows the amplitude of the reflected radar waves as a function of traveltime, which is related to the radial depth of penetration. A planar feature that intersects the borehole, such as a dipping fracture, is characterized by the chevron-shaped pattern (yellow line) in the radargram showing the upper limb (UL) and lower limb (LL) of the fracture. Sometimes only one limb of the reflector can be imaged. Reflectors do not need to intersect the borehole to be interpreted.

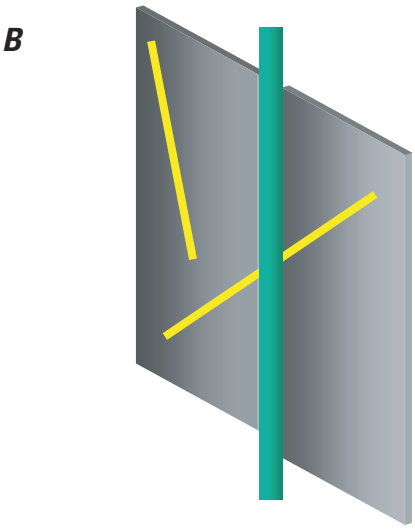

In the directional reflection mode, the reflected signal can be resolved in 36 distinct planes about the borehole. Each plane is analyzed for reflectors. Although a reflection is strongest in one plane, it may be visible in other planes as well.

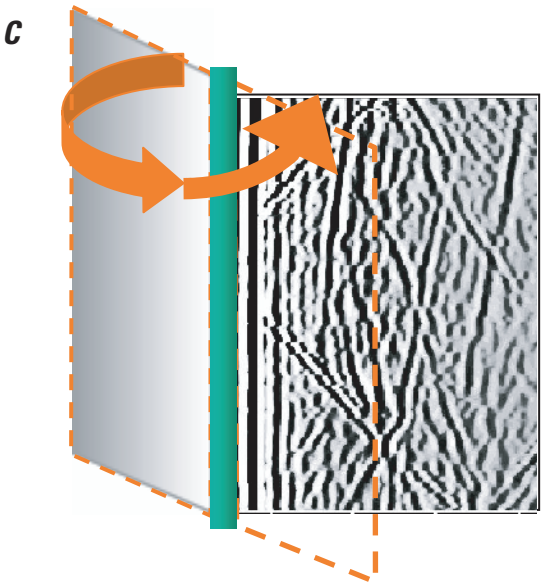

Radar results are depicted in a radargram that shows reflections from both sides of the borehole. Each plane is inspected for planar features, and their depth of intersection with the borehole and dip are determined. The reflector's in-phase and out-of-phase signatures are analyzed. Generally, in the absence of interference, the strike of a reflector can be determined. Occasionally the strike cannot be determined because of noise in the data.

Figure 3. Schematic diagrams of *A*, a borehole, an intersecting dipping fracture, and the upper and lower limbs of the fracture on a radargram; *B*, schematic of reflected radar waves resolved into a plane; and *C*, the depiction of radar results in a radargram. Figure modified from Johnson and Joesten (2005, fig. 4).

be made (fig. 3*A*). In cases where the phase of the reflector cannot be determined, the strike of the reflector can only be resolved in some direction ±180°.

The reflectors were assigned scores for each of the type of reflector, apparent continuity, and strength of the reflector in the radargram. Each reflector was assigned a type of either "UL," for upper limb, or "LL," for lower limb (fig. 3*A*). A score of 1 indicates a very good, continuous reflector and a score of 5 indicates a discontinuous, poor reflector. For some reflectors, interferences from other features preclude the determination of strike. In addition, if a reflecting feature is non-planar, it can prevent the determination of strike, dip, or point of intersection. However, the reflector's dip and the depth of intersection with the borehole can be determined, even if the strike cannot be determined. The directional confidence factor indicates the certainty associated with the azimuthal direction of the reflector (1 indicates very certain and 5 indicates almost no certainty).

Heat-Pulse Flowmeter

General heat-pulse flowmeter (HPFM) techniques are described by Paillet and others (1987) and Paillet (1998, 2000, and 2004). Flowmeter measurements were made with a Mount Sopris Instruments model HPF–2293 flowmeter. The HPFM was used with stationary measurements and a fully fit diverter that is designed to channel all of the flow through the measurement chamber of the tool, thereby capturing all vertical flow in the well.

The HPFM measurement locations were chosen in conjunction with the interpretations of the FEC, TEMP, SC, caliper, and imaging logs. HPFM measurements were collected at discrete locations, usually above and below fractures at places where the diverters would seat well in the borehole and channel the vertical flow through the measurement chamber of the tool. Multiple measurements were taken at each location to ensure that flow rates were repeatable and not transient flows, such as flow related to movement of the tool in the borehole, disturbance of the cable, or cycling of a pump on and off. Measurements were taken under ambient conditions and then under stressed conditions. The wells were stressed by pumping at low rates (about 0.5 gallons per minute [gal/min]). The upper detection limit of the HPFM is about 1 gal/min with a fully fit diverter. Methods used to collect HPFM data are described in detail by Williams and Paillet (2002).

The HPFM can detect flow rates as low as 0.010 ± 0.005 gal/min, which corresponds to a transmissivity of about 1 foot squared per day (ft^2/d). Transmissivities below that cutoff must be measured with another method, such as packer testing or fluid-replacement logging. In addition, flowmeters used in open boreholes have a dynamic resolution that can only identify zones within one to two orders of magnitude of the most transmissive zone in each borehole. Consequently, the HPFM is considered an effective tool for identifying the most transmissive fractures in a borehole, down to the detection level of the tool.

Typically, the flowmeter logs were not collected until the boreholes reached quasi-steady-state conditions. A quasi-steady-state condition is defined as a rate of change in borehole storage that is less than the resolution of the flowmeter tool.

$$Q_{SS} = \Delta Q_{BS} = \pi r2\ \Delta H/time \leq \text{resolution of HPFM}, \quad (1)$$

where

Q_{SS} is the quasi-steady-state flow rate,
ΔQ_{BS} is the change in borehole storage,
r is radius, and
$\Delta H/time$ is the change in head of the boreholes over a measured time interval.

In practical terms, *Qss* occurs when the change in the water level in a 6-inch borehole is less than 0.01 foot per minute, which is equal to 0.015 gal/min and less than the lower resolution of the HPFM tool.

If a borehole was not at quasi-steady-state conditions during flowmeter measurements, the amount of water coming from borehole storage and going directly to the pump had to be removed from the pumping rate by using the following equation:

$$Q_{stress} = (Q_{pumping\ flow\ rate} - \Delta Q_{BS}), \quad (2)$$

where

Q_{stress} is the effective stress rate, and
$Q_{pumping\ flow\ rate}$ is steady pumping flow rate.

The HPFM used in this investigation was calibrated at the factory under controlled conditions, and then checked in the field. When conditions permitted, flow was measured in the casing, which typically provides the best fit of the diverter, under known pumping conditions with a steady water level. These measurements were used to verify the performance of the tool. When necessary, the flowmeter measurements from the uncased region of the borehole were normalized to these known flow rates by using the following equation:

$$QN = Q_{stress} \times Q_{measured}/Qmax_{measured}, \quad (3)$$

where

QN is the normalized flow rate,
$Q_{measured}$ is measured flow rate, and
$Qmax_{measured}$ is the maximum flow rate, which is usually measured near the pump in the casing.

Estimates of Transmissivity and Hydraulic Characterization

Transmissivity is a measure of the ability of the aquifer to transmit water. The unit of measurement is cubic foot per day per square foot times foot of aquifer thickness $[(ft^3/d)/ft^2]ft$, which represents a volumetric flow rate over a given area for

a known thickness of aquifer. These terms simplify to the unit of foot squared per day, ft^2/d, which is used in this report. For each borehole, transmissivities were estimated for the entire open hole and for individual transmissive fractures and fracture zones within the borehole. Transmissivity values in this report should be considered estimates that are within an order of magnitude of the true borehole transmissivity.

Specific Capacity and Estimates of Transmissivity by Open-Hole Tests

Open-hole transmissivity was estimated by using a method described by Bradbury and Rothschild (1985) by using the water-level decline in response to pumping. The storage coefficient was assumed to be 0.0005, and no well-loss coefficient was used (Todd, 1980). These methods were used as a check of the results obtained through modeling of the HPFM data with Flow-Log Analysis of Single Holes (FLASH) (Day-Lewis and others, 2011).

In addition, another method that uses specific capacity to estimate transmissivity was used for comparison. Transmissivity was estimated by using an empirical equation that relates transmissivity to the rate of water-level decline under a fixed discharge rate:

$$T = C \times (Q \text{ measured}/s)^a, \quad (4)$$

where

- T is the transmissivity,
- C is constant, set equal to 0.33 for metamorphic and crystalline rock,
- Q is the measured pumping rate in cubic meters per minute,
- s is the change in head in response to pumping in meters, and
- a is a power, set equal to 1.30 for metamorphic and crystalline rock.

The parameters C and a were derived for metamorphic and crystalline rock (table 1 in Srivastav and others, 2007) in metric units, and the results were converted to English units. This approach does not require the additional parameters of pumping duration, storage coefficient, and aquifer thickness.

Quantitative Analysis of HPFM Data Using FLASH

A Microsoft Excel-based utility, FLASH, was used to model the flowmeter results and estimate the depth-dependent transmissivity and head of the fractures in the boreholes (Day-Lewis and others, 2011). FLASH is a graphical user interface (GUI) embedded in Microsoft Excel and is used to calibrate the analytical borehole flow model with estimated values for flow-zone transmissivity and far-field heads. The FLASH solution is based on a radial flow analytical solution which assumes the following to solve a series of Thiem equations: (1) steady-state radial flow to the borehole, (2) an isotropic homogeneous layer or fracture, and (3) either a fixed radius of influence (ROI) or transmissivity.

FLASH uses an interpretation of the measured flow regimes, the input data, and either an estimate of ROI or total-hole transmissivity to solve for the other. Vertical flow rates are simulated between discrete intervals and are compared to interpreted profiles of flow. Estimates of zone transmissivity and head are iteratively changed for a manual solution. Alternately, the program has the option of using the Solver package in Excel for an automated calibration that minimizes the sum of squared errors (SSE) between the observed and simulated flow profiles. Three optional constraints are available to regularize the Solver solution. The maximum head difference and (or) the minimum transmissivity factor can be used. In addition, a weighting factor can be put on the regularization for head differences, whereby a larger weighting value causes a "flatter profile" or a smaller head difference from zero. Collectively these constraints are intended to prevent a numerical solution with unrealistic values.

Well information is entered in the upper left section of the FLASH GUI (fig. 4) and includes the elevation of the measuring point, number of fractures to be modeled, well diameter, drawdown, and depth to water under ambient conditions. This section provides basic input for the Thiem equation calculations and also serves as documentation for the model. For the initial run, a transmissivity and radius of influence (ROI) were entered. For each well, two models were run—one with the ROI assumed at 50 ft and the other at 100 ft. A fixed ROI was assumed for all wells so that the estimates of transmissivity are comparable between boreholes, which is similar to the approach taken by Shapiro and Hsieh (1998). The actual ROI varies for each fracture, but in the FLASH model it is represented as a single uniform value. The estimate of transmissivity is fairly insensitive to changes in ROI; increasing the ROI by a factor of 10 causes roughly a doubling of the transmissivity. ROI values of 50 and 100 ft were used for all boreholes, and the transmissivity values generated by this method were compared to transmissivity values determined with another method to verify that the results were within an order of magnitude.

The depth of the fractures is entered on the far left side of the program display (fig. 4) along with the interpretation of the ambient and pumped ("stressed") flow profiles ("Flow above layer bottom depths" in fig. 4). On the right side of the display, the interpreted flow profiles (in bold dashed lines) are plotted over the point data from HPFM measurements in the field. When there is scatter in the point data, the line indicating the interpretation of flow is fitted through the points. For example, when there is poor seal and some flow bypasses the measurement chamber, the interpreted flow profile is fit to the higher flow rate measurements assuming the reduced flow rate is attributed to minor bypass. During processing, initial estimates of transmissivity and head were entered for each fracture. If

REQUIRED INPUT:

Wellname: **Tylerville 77LMR**

Elevation of measuring point [FT]	7.8
Number of flow zones [-]	4
Well diameter [IN]	6
Drawdown [FT]	0.25
Depth to ambient water level [FT]	5.75
Top of plot [FT]	135
Depth at bottom of well [FT]	343.5
Radius of influence (R_0) [FT]	100.0
Total transmissivity (T_{total}) [FT²/day]	367.13

Run Solver

- Estimate Transmissivity
- Estimate ROI
- Solve without Regularization
- Solve with Regularization

ABS (del h) maximum	5.00E+00
Regularization weight	1.00E-04
Tfactor minimum [-]	1.00E-09

Flow above layer bottom depths

FRACTURES	Bottom Depth [FT]	Ambient [GPM]	Stressed [GPM]	Tfactor [FT²/D]	Del h [FT]	Farfield head [FT]
4	156.00	0.00	0.50	0.14	0.00	2.07
3	193.00	0.00	0.43	0.16	0.00	2.07
2	310.00	0.00	0.35	0.30	0.00	2.07
1	331.00	0.00	0.20	0.40	0.00	2.07

SIMULATED PROFILES (DO NOT EDIT)

MSE [GPM²]	2.04E-13	Sum T_{factor}	1.000	Sum del h^2	0.00
Ambient WL [FT]	2.07	Estimated Ttotal [FT²/day]	367.125	Regularized Misfit	0.00
Pumped WL [FT]	1.82				

FRACTURES:	Depth [FT]	Ambient Flow above [GPM]	Stressed Flow above [GPM]	Ambient Error [GPM]	Stressed Error [GPM]	Zone T [FT²/day]	Fraction of total transmissivity
4	156.00	0.000	0.500	0.000	0.000	51.398	0.140
3	193.00	0.000	0.430	0.000	0.000	58.740	0.160
2	310.00	0.000	0.350	0.000	0.000	110.137	0.300
1	331.00	0.000	0.200	0.000	0.000	146.850	0.400

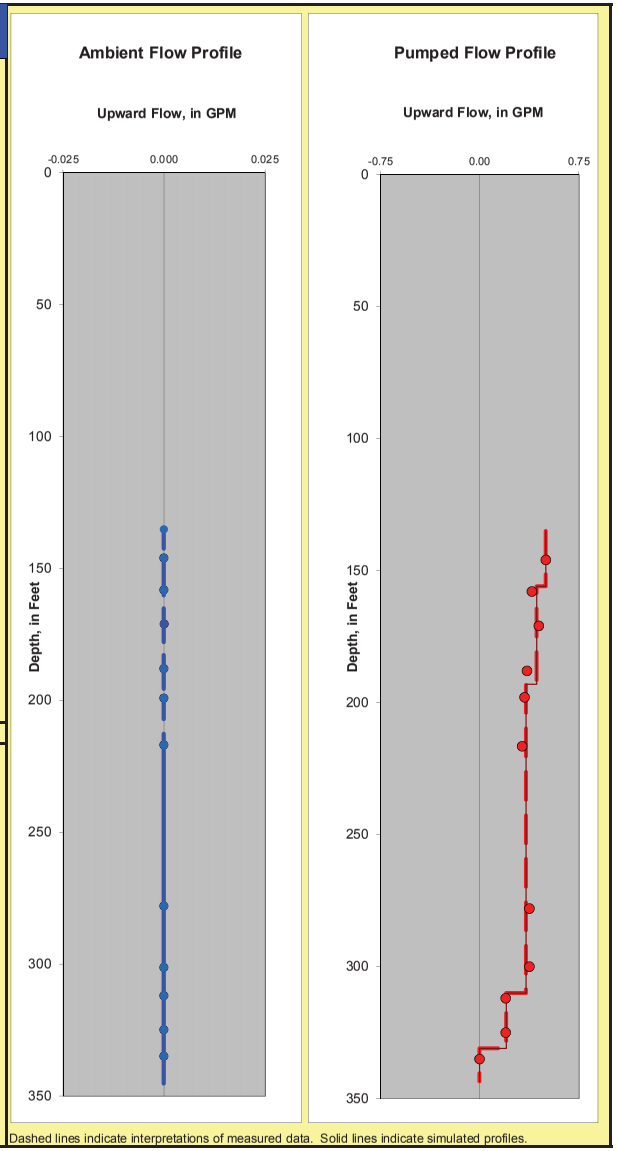

Dashed lines indicate interpretations of measured data. Solid lines indicate simulated profiles.

Notes: FT = Feet; IN = Inches; ROI = Radius of influence; ABS = Absolute value; GPM = Gallons per minute; WL = Water level; MSE = Mean squared error

Figure 4. Example input and output from Flow Log Analysis of Single Holes (FLASH), the utility for modeling flowmeter data. Example provided for borehole 77–LMR in Tylerville, Connecticut.

no ambient flow was measured, the differences in heads were entered as 0. If ambient flow was measured, the heads were adjusted manually to drive water from the higher head fracture to the lower head fracture, and estimates for transmissivity were entered for each fracture or zone.

A visual inspection of the fit is provided with the graph. The simulated flow profiles are automatically plotted in FLASH (as thin solid lines) over the interpreted profiles (dashed lines). In addition, statistical measures of the fit are provided in the lower left section. Once data, interpretation profiles, and initial model parameters are entered, the Theim equation is computed for each depth, and discrete-interval transmissivity, head, and statistical parameters are updated automatically. Once a reasonably good fit was obtained by manually adjusting the transmissivity and head for each depth, the solver solution was used to measure a transmissivity with a fixed ROI. The table on the lower left side of the page shows the output from FLASH. An estimate of the solution fit is provided with the SSE in gallons per minute squared $(gal/min)^2$. A table in the output section shows the discrete zone transmissivity and the percent transmissivity for each fracture zone in the model.

Data and Results by Well

Data are summarized in the following subsections for each of the wells in the Tylerville study area. The data for individual wells are provided in appendixes. Appendixes 1–6 contain the data for the six wells that were logged with the complete suite of tools. Appendix 7 has the data for 95–BR, which includes caliper, fluid conductivity, and temperature data only. In the following subsections, the results for each well are summarized in the categories of "borehole location and construction," "lithologic characterization," "fracture characterization," "hydraulic characterization," and "borehole radar."

"Borehole location and construction" includes information on the location and completion of the well and its physical condition at the time of logging (figure *x*–1 in each appendix, where *x* is the appendix number). Each well is described in terms of the total depth of the well, the amount of casing aboveground and belowground, and the measurement point that was used for geophysical logging. The deviation data is plotted in plan view (or as a "bull's eye" plot) and in a cross section. The plan view plot shows the well head at the center of the plot, and the borehole location is plotted as a function of depth with respect to true north. The cross-sectional plot shows the depth along the bearing in the direction of the borehole deviation. These plots are shown in figure *x*–2 in each appendix, and the tilt and azimuth data that the plots are based on are shown in figure *x*–3 of each appendix.

In "lithologic characterization," a general description of the rock type is summarized for the well on the basis of the standard geophysical logs and imaging logs shown in figure *x*–3 in each appendix. Data include natural gamma, EMI, ATV, OTV, and interpreted-structure logs. The rock types observed in the image logs are also described.

"Fracture characterization" includes a summary of all fractures observed in the borehole. In this investigation, the term "fracture" refers to a planar discontinuity in the rock. Fractures are described as major fractures, minor fractures, sealed fractures, or transmissive fractures. The term "transmissive fracture" indicates a single fracture that was identified with the HPFM as transmitting water under ambient or pumped conditions. The terms "fracture zone" and "transmissive zone" refer to zones of the borehole or rock that have multiple fractures. Fractures were identified by using the caliper, ATV, and OTV logs (figure *x*–3 in each appendix). Fractures and other structural features (such as foliation, banding, and felsic layers) are shown in projection plots, tadpole plots, and stereographic projections (stereoplots) (figure *x*–4 in each appendix). The interpreted structures are shown as projection plots that overlay the televiewer images, which are a flattened image of the borehole wall that has been split along north (fig. 5). Thus, in the projection plot, fractures can be traced directly over the image. Planar features appear as sine waves from which strike and dip can be determined (Williams and Johnson, 2004). The same structural features are also shown in tadpole plots. In the tadpole plot, the depth of the planar feature is shown on the y-axis (fig. 5*A*). The dip of the feature is shown on the x-axis (from 0–90°, with 0 horizontal and 90 vertical). The tail of the tadpole points in the direction of dip (strike + 90°) relative to an imaginary compass with true north at the top of the page. In these plots the structural features have been corrected for deviation and magnetic declination. Planar features are also shown in stereoplots, where the pole to the plane of a feature is projected from a lower hemisphere to an equatorial plotting surface (figs. 5*A* and 6). A stereoplot reduces each planar feature to a point that represents the intersection of a pole that is perpendicular to the plane. Hence, the points on the plotting circle, which represents the equatorial plane of the hemisphere, are called "poles to planes" (fig. 6). In this type of plot, a nearly horizontal fracture would have a pole that projects near the center of the stereoplot. The pole of a steeply dipping fracture would project near the outside edge of the stereoplot and would be located on the side of the circle opposite from the direction of dip (fig. 6*B*). The stereoplots provide a graphical method for assessing the clustering or variability of the poles to planes. The structural interpretations are also provided in tables (table *x*–1 in each appendix).

"Hydraulic characterization" includes plots of FEC, TEMP, and SC logs that were examined for deflections in the data and vertical sections of the well where the FEC and TEMP were constant, which suggests vertical flow within the well. The FEC, TEMP, and SC logs are also shown in differencing mode for the ambient and postpumping conditions to observe where the water columns changed in response to pumping. These logs are shown in figure *x*–5 of each appendix. In addition, the flowmeter logs collected under ambient

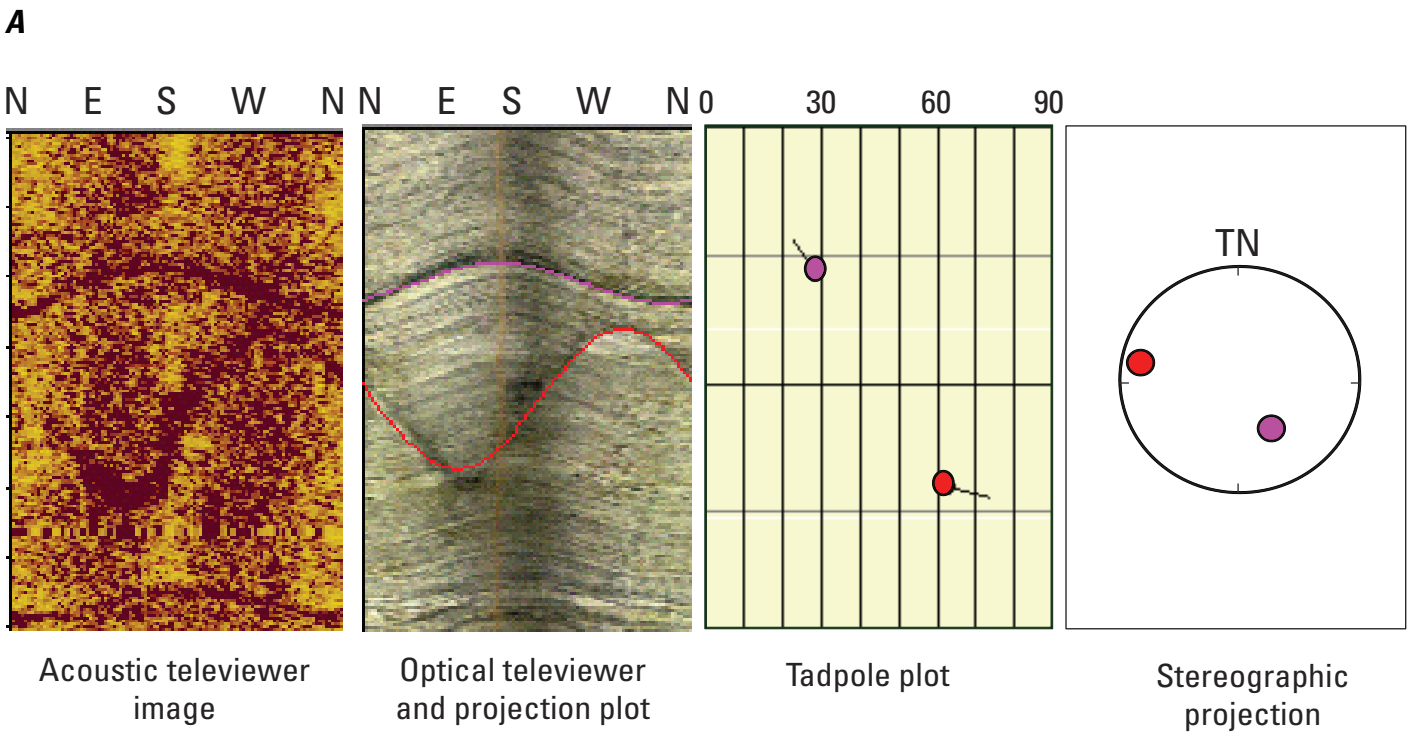

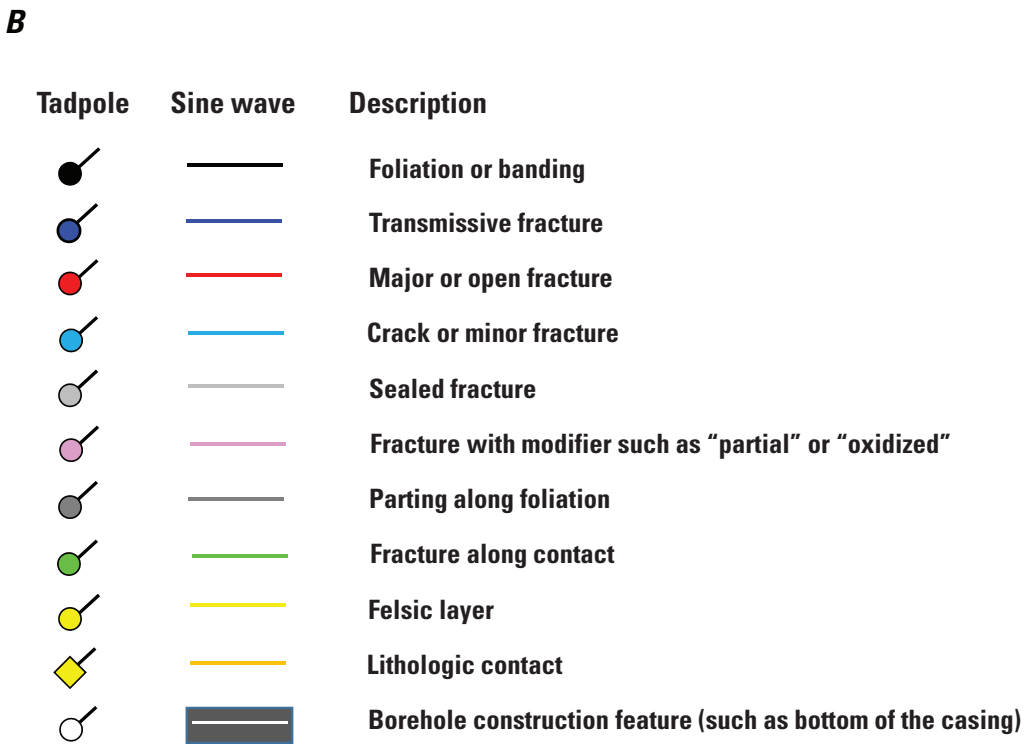

Figure 5. *A*, Acoustic and optical televiewer data, and interpretation of features shown in three types of structure plots, including a projection plot that shows the trace of the feature on the image, a tadpole plot that shows strike, dip, and depth of features, and a stereographic projection that shows the strike and dip of features. *B*, Color codes and symbols used in the structure plots. TN, true north.

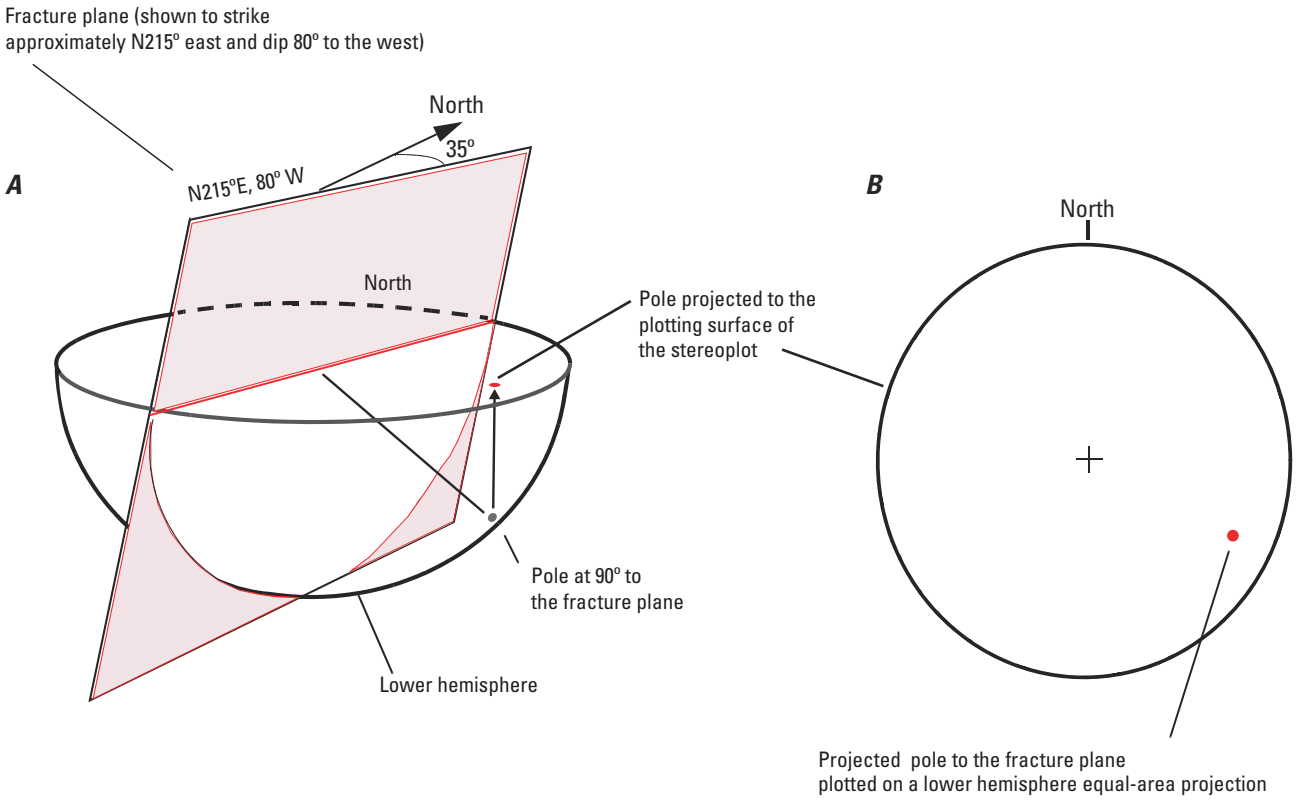

Figure 6. Schematic diagrams of a stereographic projection, showing *A*, a lower hemisphere intersected by a fracture plane and *B*, a stereoplot, in which the orientation of the fracture plane is reduced to a point by plotting the pole to the plane on a lower hemisphere and projecting it up to the plotting surface. In this investigation, all fractures were oriented relative to true north. Figure modified from Johnson and others (1998, fig. 11).

and pumped conditions are shown next to the FEC and TEMP logs. HPFM data show the measured vertical flow rate on the x-axis in gallons per minute and depth in feet on the y-axis. Together these measurements can help identify zones contributing water to the wells under ambient and pumped conditions. Blue points indicate flows that were measured under ambient conditions, and red points indicate flows measured under pumping conditions. Solid lines indicate the interpreted flow profiles under ambient and pumping conditions. The ambient and pumped profiles, along with ambient and pumped water levels, were simulated by using FLASH to determine the head and transmissivity of the discrete zones that were modeled. The interpretation of the flowmeter data is described in the text, and the results of modeling using FLASH are shown in figure *x*–6 in the appendix for each borehole. In addition, the modeled head and transmissivity of the fractures/fracture zones are provided in tables within the text of the report.

"Borehole radar" summarizes nondirectional data and directional data. Plots of nondirectional radar data and direct-arrival analysis are included in figure *x*–7 in the appendixes. These plots include logs for traveltime to first arrival, velocity, dielectric permittivity, peak-to-peak amplitude (at the first arrival), and an estimate of attenuation. Zones of low velocity and increased attenuation, which are indicators of water-filled fractures, are discussed in the "borehole radar" sections and compared to transmissive zones identified with the HPFM.

For the directional radar data (figure *x*–8 in each appendix), the interpretations of radar reflectors are displayed in projection plots, tadpole plots, and stereoplots. All results are shown oriented to true north. Because some of these reflectors can project to above or below the open section of the boreholes, the well construction is provided next to the interpretation. For the radar plots, a modified tadpole plot was used (fig. 7). The tadpole plot for the radar reflectors uses a color code and modified tadpoles to describe the reflectors (fig. 7*A*). The interpretations of the reflectors are also provided in tables (table *x*–2 in each appendix). Collectively, these plots can be used to help assess the spatial distribution and variability of data that have orientations, such as fractures and radar reflectors.

A summary of all well location and construction, log collection, and calibration information for each well is provided in figure *x*–1 in the appendix for the well. This header is included as text in the ASCII data files. The text files are

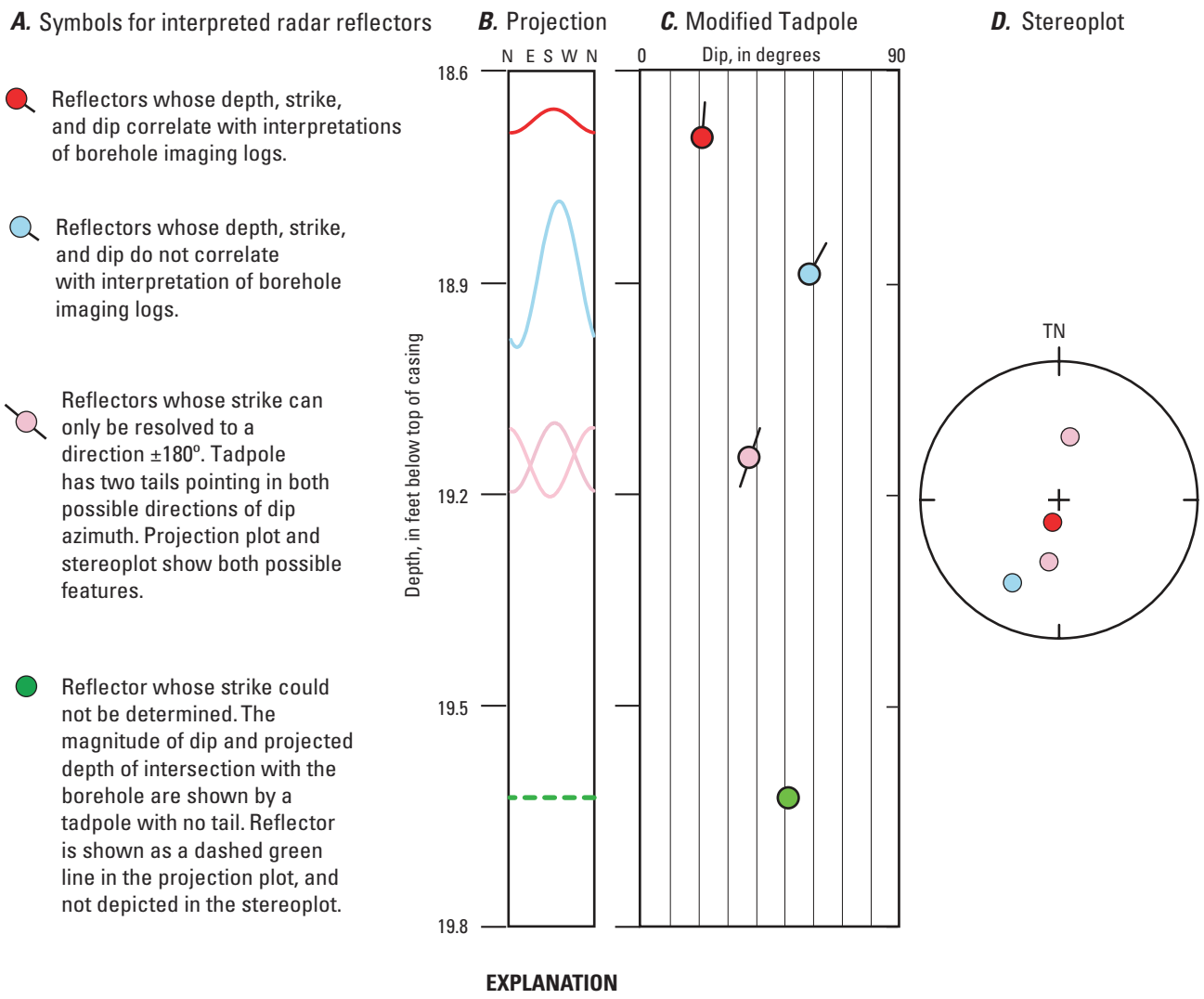

EXPLANATION

A. **Symbols (and colors) used in this investigation**—Represent the planar features identified in borehole-radar logs

B. **Projection plot**—Shows where the radar reflectors are projected to intersect the borehole. Depth of projected intersection is plotted along the y-axis. The bottom of the sine wave indicates the dip azimuth relative to true north (TN), which is shown along the x-axis

C. **Modified tadpole plot**—Depth is plotted along the y-axis and the magnitude of dip is plotted on the x-axis. The tail of the tadpole points in the direction of dip relative to magnetic north, which is at the top of the page

D. **Stereographic projection plot**—Poles to the planar features are shown in a lower-hemisphere equal-area stereonet for features where strike and dip could be determined

Figure 7. Graphic representation of interpretation of single-hole radar reflectors. *A*, Symbols and colors used in this investigation. *B*, Projection plot, *C*, Modified tadpole plot, and *D*, Stereographic projection plot. Figure modified from Johnson and Joesten (2005, fig. 6).

formatted in LAS2, Log ASCII Standard, version 2.0 (Canadian Well Logging Standard, www.cwls.org). For more details on the format of the ASCII logs, see http://www.cwls.org/wp-content/uploads/2014/09/LAS_20_Update_Jan2014.pdf.

Files that cannot be exported to ASCII data have been published in portable document format (PDF) for viewing and (or) printing. In addition, data in WellCAD file format (*.wcl) are available upon request, which can be opened with WellCAD Reader or with a licensed version of WellCAD to explore the images directly. WellCAD Reader can be downloaded free from http://www.alt.lu/downloads.htm.

Borehole 1640–SR

Borehole location and construction.—1640–SR is a production well at the State of Connecticut Department of Transportation facility at 1640 Saybrook Road (fig. 1, table 1). It was drilled in 1993 to provide water for the facility and was rated at the time of installation with a driller's yield of 3.0 gal/min. The well was logged from June 21 to 25, 2014. Borehole information and geophysical logging history are shown in appendix 1 (fig. 1–1). Geophysical logs and results are shown in appendix 1 (figs. 1–2 through 1–8, tables 1–1 and 1–2).

The steel casing extends from 1.27 ft above land surface to a total depth of 144 ft bTOC. The well was completed to a total depth of 501.4 ft bTOC (500 ft below land surface). Borehole deviation logs indicate 1640–SR deviates a total of about 14.3 ft toward the north (appendix 1, fig. 1–2). The ambient water level at the time of logging was 60.6 ft bTOC on June 21, 2014.

Lithologic characterization.—The borehole image, gamma, and EMI logs indicate the lithology is fairly uniform, with minor variations over the depth of the borehole. EMI conductivity logs indicate the rocks are fairly resistive. Borehole imaging logs and conventional logs are shown in appendix 1 (fig. 1–3). The OTV images indicate the rock type is a calc-silicate gneiss with felsic layers that are either pegmatites or felsic portions of the gneiss. The upper part of the borehole (from a depth of 144 to 200 ft bTOC) is reddish-orange-brown in color, which suggests the rock is iron stained or the water is oxidized and turbid. From 300 to 430 ft, the rock is dark greenish gray, fine grained with foliated layers, with lighter greenish-gray equigranular layers. Below 430 ft, there are more felsic, medium-grained, equigranular layers consistent with a banded gneiss. Foliation generally strikes N. 150° E. and dips gently (17°) toward the southwest (appendix 1, fig. 1–4, table 1–1). Lithologic layers identified in the images appear to be parallel to the foliation, with a few of the contacts nearly orthogonal to the foliation. The lithologic contacts (yellow, in appendix 1, fig. 1–4) strike at an average of TN. 94° E. and dip less than 10° toward the south. In general, the foliation, banding, and felsic contacts are fairly flat lying.

Fracture characterization.—The orientations of all fractures identified in the OTV and ATV logs are provided in figures and tables (appendix 1, fig. 1–4, table 1–1). Numerous fractures were interpreted from the borehole images. Four fractures (shown in red in the projection plot, tadpole plot, and stereoplot in appendix 1, fig. 1–4) appear to be parallel to the foliation. Minor fractures (light blue in appendix 1, fig. 1–4) are generally parallel to the foliation and the lithologic contacts. They strike on average TN. 135° E. and dip gently 8° to the southwest. An inflow zone was identified at depths from 322 to 324 ft bTOC, and flow was attributed to four transmissive fractures. Two of the fractures dip to the northeast (averaging a strike of TN. 306° E.), and two dip to the west (averaging a strike of TN. 189° E.). The northeast-dipping fractures have an average dip of 20°, and the west-dipping fractures have a slightly steeper dip of 33°.

Hydraulic characterization.—The FEC, TEMP, and SC logs for 1640–SR indicate the possibility of ambient vertical flow from the near the bottom of casing to a total depth of 452 ft bTOC (appendix 1, fig. 1–5). But HPFM methods could only confirm downflow to a depth of 320 ft bTOC. Minor downflow was measured with the HPFM under ambient conditions from the bottom of casing or a minor fracture at a depth of 146.5 ft to the fractures at a depth of about 324 ft bTOC. On June 23, 2014, 1640–SR was hydraulically stressed by pumping from the top of the borehole at a rate of 0.55 gal/min, which imposed a water-level decline of 5.1 ft in the same hole. The water that was pumped from the borehole was rusty, copper brown, and turbid. The flowmeter measurements were collected after the borehole reached quasi-steady state conditions after about one hour of pumping. The specific capacity of the open borehole was 0.11 gallon per minute per foot (gal/min/ft) of drawdown. Using the methods of Bradbury and Rothschild (1985), the open-hole transmissivity was estimated at 20.5 ft^2/d. Using the methods of Srivastav and others (2007), the transmissivity was estimated at 8.6 ft^2/d.

FLASH was used to model zone head and transmissivity. Three zones were included in the model. They are at depths of 144 ft (base of casing), 324 ft (a fracture zone), and 452 ft (a single fracture). The flow measurements and the simulated flow profiles are shown in appendix 1 (fig. 1–6). A ROI of 100 ft was assumed, and the transmissivity was computed. The head and transmissivity of each fracture zone is listed in table 2. The final solution of the FLASH model produced an open-hole transmissivity of 19.8 ft^2/d (appendix 1, fig. 1–6). The SSE was 3.0E-14 $(gal/min)^2$, which indicates a good fit of the simulated results compared to the observed flowmeter data. Results are summarized in table 2 and appendix 1 (fig. 1–6). In this interpretation, 85 percent of the water was determined to come from the bottom of casing or the minor fracture at 146.5 ft bTOC. In addition, fractures at a depth of about 324 ft contribute 11 percent to the transmissivity of the borehole, and the fracture at 452 ft bTOC accounts for 4 percent of the transmissivity.

Table 2. Hydrologic analysis of flow in borehole 1640–SR, in the Tylerville study area, Haddam, Connecticut.

[Radius of investigation = 100 feet (ft). ft²/d, foot squared per day; TOC, top of casing]

Depth of transmissive zone, in ft	Ambient flow above transmissive zone, in ft	Pumped flow above transmissive zone, in ft	Zone transmissivity, in ft²/d	Depth to water level, in ft below TOC	Water level elevation, in ft	Percent of total transmissivity
144.00	0.00	0.55	17.0	60.50	4.00	85
324.00	-0.01	0.07	2.1	59.63	3.13	11
452.00	0.00	0.02	0.7	60.39	3.89	4

Borehole radar.—The 250-MHz nondirectional dipole data were analyzed for direct-wave arrival time and attenuation to identify zones of relatively low velocity and high attenuation, which are consistent with the presence of water-filled fractures. Analysis of the direct wave indicates the presence of zones of relatively low velocity at depths of 172 to 178, 200 to 209.5, 216 to 221.4, 244 to 250, 274 to 280, 302 to 307, 346 to 359, 410 to 413, and 453 to 460 ft bTOC (appendix 1, fig. 1–7). For each of these low-velocity zones, the radar images had an associated increase in attenuation and increase in dielectric permittivity, which is inversely proportional to the velocity. Only a minor decrease in velocity (compared to other low-velocity zones in the borehole) and a decrease in attenuation were identified at the transmissive zone at a depth of 322 to 324 ft. The nondirectional radar, first arrival, velocity, dielectric permittivity, amplitude (at the first arrival), and attenuation data are shown in appendix 1 (fig. 1–7).

An average velocity of 394.4 ft/µs was used to interpret the reflectors in the 60-MHz directional radar data (appendix 1, fig. 1–8). The depth and orientation of the features are shown in a projection plot, a tadpole plot, and a stereoplot. A total of 25 features were identified in the radar images. All features are shown in plots and listed in appendix 1 (fig. 1–8, table 1–2). Most of the reflectors had scores that indicate poor to moderate conductivity and poor to moderate confidence in their strike. Two thirds of the features have moderate dips (30 to 60°). They predominantly strike to the southeast and have a dip azimuth to the south-southwest. The other third of the reflectors have shallow dips. These features have different directions, but the majority dip to the south-southwest.

Six of the reflectors correlate with features identified by the ATV and OTV logs at midpoint depths of 146.3, 191.9, 246.1, 260.2, 322.2, and 389.8 ft bTOC (appendixes fig. 1–4, fig. 1–8). Two reflectors correlate with transmissive fractures. One reflector projects to 146.3 ft, which is near the base of casing and at a similar depth as a nearly horizontal fracture observed in the image logs at a depth of 146.5 ft bTOC. The reflector at a depth of 246.1 ft is coincident with the foliation of the rock. The reflector at 389.8 ft bTOC coincides with a lithologic contact at a depth of 389.9 ft bTOC. Two other features at midpoint depths of 191.9 and 260.2 ft bTOC coincide with minor-looking fractures in the borehole image logs.

Sixteen reflectors do not coincide with features in the image logs. These reflectors (shown in light blue in appendix 1, fig. 1–8) generally strike to the east and dip gently toward the south (with an average orientation of TN. 179° E., dipping 16°). A total of six reflectors project to intersect the borehole above or below the open section of the borehole. Four reflectors project to behind the casing. Two weak reflectors project to below the bottom of the open borehole at depths of 502.6 and 503.0 ft bTOC. The radar images and the stereoplot of the interpreted reflectors indicate that these features are fairly continuous in the rock surrounding the borehole and are more steeply dipping than the features observed in borehole imaging.

Borehole 76–BR

Borehole location and construction.—76–BR is a domestic well that was drilled at 76 Bridge Road (fig. 1, table 1). No drilling records exist for this well. The steel casing extends from 1 ft above land surface down to a total of 151.3 ft bTOC. Well 76–BR was completed to a total depth of 301 ft bTOC. 76–BR was logged on July 29 and 30, 2014. Borehole information and geophysical logging history are shown in appendix 2 (fig. 2–1). All measurements are referenced to the top of casing. Geophysical logs and results are shown in appendix 2 (figs. 2–2 through 2–8, tables 2–1 and 2–2).

Borehole deviation logs indicate 76–BR is nearly vertical. It deviates a total of 1 ft toward the northwest (appendix 2, fig. 2–2). The ambient water level at the time of logging was 85.0 ft bTOC.

Lithologic characterization.—The ATV, EMI, and gamma logs show little variation over the depth of the borehole, suggesting a fairly uniform rock (appendix 2, fig. 2–3). Borehole imaging logs and conventional logs indicate the rock type is gneiss. Minor variations in the rock can be seen in the OTV. The rock in the OTV images at depths of 220 to 255 ft appear to be fairly dark and fine grained. A prominent felsic zone is evident from about 256 to 270 ft bTOC. Below 270 ft the rock appears to be banded. Other felsic bands occur at depths of about 188, 206.4, 228.8, 276, and 295 ft bTOC (appendix 2: fig. 2–3, fig. 2–4, table 2–1). Foliation and banding of the

gneiss strike at average orientations of TN. 95° E. and 187° E. and have shallow dips less than 10° (to the south and west).

Fracture characterization.—The caliper log shows enlarged diameter sections of the borehole at depths of 185, 239, and 243.5 ft bTOC, which suggests the presence of fractures (appendix 2, fig. 2–3). The orientations of all fractures identified in the OTV and ATV logs are provided in figures and tables (appendix 2, fig. 2–4, table 2–1). All of the fractures identified in image logs of 76–BR have shallow dips (less than 30°). Most of the fractures dip northeast with an orientation of TN. 330° E., dipping 18°. The transmissive fractures were identified at depths of about 152, 182, 240, and 291 ft bTOC. The orientations of these transmissive fractures at depths of about 240 and 275 ft bTOC strike toward the northwest and dip toward the northeast. The fractures at depths of 238 and 291 ft bTOC strike gently toward the south-southeast and dip toward the west-southwest.

Hydraulic characterization.—HPFM logs collected on July 30, 2014, indicate that no ambient flow was measured at the time of logging (appendix 2, fig. 2–5). Under a pumping rate of 0.5 gal/min, the water level declined a total of 18.7 ft. The specific capacity of the open hole was 0.02 gal/min/ft of drawdown, indicating that little water is produced per foot of drawdown. By using the methods of Bradbury and Rothschild (1985), the open-hole transmissivity was estimated at 3.2 ft^2/d. By using the empirical equations for specific capacity, the transmissivity was estimated at 1.0 ft^2/d (Srivastav and others, 2007). These methods provide consistent results and indicate that this is not a highly transmissive borehole.

A comparison of the FEC, TEMP, and SC logs collected before and after pumping suggest there is inflow to the borehole at depths of about 160, 188, 242, and 291 ft bTOC. At close inspection, even the minor inflow from the fracture at 291 ft can be seen in the SC log. These inferences from the differenced fluid logs were confirmed with the HPFM. No ambient flow was measured with the HPFM, but under a pumping rate of 0.5 gal/min, water entered the borehole at 152, 184, 240, and 291 ft bTOC.

The ambient and pumped profiles were simulated by using FLASH. The simulated results produced a solution that had an SSE of 2.5E-11 $(gal/min)^2$ (appendix 2, fig. 2–6). The fracture near the bottom of casing at 152 ft accounted for 12 percent of the total transmissivity. The fracture zone at 184 ft accounted for 63 percent of the transmissivity. The fractures at 240 and 291 ft bTOC accounted for 12 and 13 percent, respectively. The head and transmissivity of each fracture zone is listed in table 3.

Borehole radar.—The 250-MHz, nondirectional radar data were used to determine the direct-wave arrival time, which along with the presence of reflectors is used to infer locations of water-filled fractures. The nondirectional radar in 76–BR is characterized by low-velocity zones at depths of 160, 184 to 196, 206 to 208, and 240 to 248 ft bTOC (appendix 2, fig. 2–7). These zones were also characterized by reflections in the radargram. The zones around depths of 160, 185, and 240 ft bTOC are coincident with zones that were identified as transmissive fractures.

An average velocity of 396.7 ft/μs was used to process the directional data from 76–BR. A total of 16 reflectors were interpreted from the 60-MHz directional data. Several strong reflectors can be seen in the radar plots. Three of the reflectors project to the casing (appendix 2, fig. 2–8, table 2–2). Their projected intersections are at depths of about 23, 120, and 133 ft bTOC. Four other reflectors project to intersect below the bottom of the borehole at depths of 327, 334, 364, and 373 ft bTOC. Most of the reflectors have shallow dips (less than 30°). Only three of the reflectors coincide at the same depth and orientation as features in the borehole logs (plotted red in appendix 2, fig. 2–8)—these are the reflectors at depths of 188, 215, and 236 ft bTOC. One very strong reflector (with continuity scores = 1) projects to the bottom of the well with a strike and dip of TN. 296° E., 22° (dipping to the northeast). This feature was deeper than what could be imaged with the OTV and ATV tools and could not be confirmed in the borehole.

The stereoplot of radar reflections (appendix 2, fig. 2–8) provides some insight into the fractures surrounding 76–BR. Stereoplots for the image plots for 76–BR are generally shallow dipping (appendix 2, fig. 2–4). But the reflectors identified in the radar plots (appendix 2, fig. 2–8) are more steeply dipping than the features observed in the boreholes.

Table 3. Hydrologic analysis of flow in borehole 76–BR, in the Tylerville study area, Haddam, Connecticut.

[Radius of investigation = 100 feet (ft). ft^2/d, foot squared per day; TOC, top of casing]

Depth of transmissive zone, in ft	Ambient flow above transmissive zone, in ft	Pumped flow above transmissive zone, in ft	Zone transmissivity, in ft^2/d	Depth to water level, in ft below TOC	Water level elevation, in ft	Percent of total transmissivity
152.00	0.00	0.50	0.6	85.00	-8.00	12
184.00	0.00	0.44	3.1	85.00	-8.00	63
240.00	0.00	0.12	0.6	85.00	-8.00	12
291.00	0.00	0.06	0.6	85.00	-8.00	13

Borehole 85–BR

Borehole location and construction.—85–BR is a domestic well located at 85 Bridge Road (fig. 1, table 1). There are no records for the construction of this well. 85–BR appears originally to have been a 3-ft-diameter dug well that was converted to a bedrock well by drilling through the bottom of the dug well. The 6-inch-diameter steel casing is approximately 3.5 ft below the top of the 3-ft-diameter cement casing. It also appears that the dug well was filled with gravel to about 4 ft below the top of cement casing and about a half a foot below the top of steel casing. This well was logged on July 30 and 31, 2014. Borehole information and geophysical logging history are shown in appendix 3 (fig. 3–1). Geophysical logs and results are shown in appendix 3 (figs. 3–2 through 3–8, tables 3–1 and 3–2).

All logs were referenced to a measuring point at the top of the 3-ft-diameter cement casing on the south side of the well. It was difficult to determine where the land surface intersected the cement casing, given that the well is on a slope with the land surface above and below the top of cement casing. Hence all log measurements are referenced to this measurement point, which can be considered to be at land surface.

The bottom of steel casing is at 141 ft below the measuring point, and the total depth of the well is 230 ft below the measurement point on the cement casing. Borehole deviation logs indicate that 85–BR is essentially vertical (appendix 3, fig. 3–2). It deviates less than 1 ft from vertical. The ambient water level was 62.5 ft below land surface. Observations made at the time of logging indicate water pumped from the well smelled like gasoline. In addition, the water was blackish and turbid. The turbidity cleared up a little, but the smell of gasoline continued during pumping.

Lithologic characterization.—The gamma tool, which can sample through the steel casing, shows a change in the natural gamma emissions at a depth of 132 ft, suggesting that this is the depth to rock (appendix 3, fig. 3–3). The gamma, EMI, and imaging logs in the open hole are fairly constant, indicating a fairly uniform rock type (appendix 3, fig. 3–3). The OTV shows a banded gneiss with fine-grained, dark greenish-gray layers with minor amounts of greenish-gray, medium-grained, equigranular felsic layers. There are also some thin layers of medium-grained felsic units, some of which appear as discontinuous lenses that are likely felsic boudins (examples in the OTV images at depths of 172.4, 176.2, 177.7, 204.0, 211.6, and 225.8 ft bTOC). The presence of boudins (felsic layers with variable thickness that appear as light-colored eye-shaped or sausage-shaped units) is consistent with the Hebron Gneiss. The average strike and dip of the foliation (dark gray in the projection plot, tadpole plot, and stereoplot in appendix 3, fig. 3–4) was TN. 310° E., with a 3° dip to the northeast. Partings along the foliation and layering (light gray in the figure) have an average strike and dip TN. 342° E., with a shallow dip 13° to the east northeast.

Fracture characterization.—The OTV and ATV images were interpreted together. Results are shown in the form of a projection plot, a tadpole plot, and a stereographic projection (appendix 3, fig. 3–4). Open fractures were identified at depths of about 148, 156, 205, and 219 ft bTOC. All of the major fractures are shallow dipping. Two of the major fractures strike to the east-southeast and dip toward the south-southwest; one strikes to the southwest and dips toward the northwest, and the other strikes north and dips toward the east. ATV and OTV indicate a few minor fractures in the borehole. Three transmissive fractures were identified in 85–BR and are tightly clustered with an average strike of TN. 351° E., 21° (northeast). Five minor fractures (appendix 3, fig. 3–4) appear to be similar in orientation to foliation and layering.

Hydraulic characterization.—Typically, temperature increases with depth. However, in 85–BR there is a thermal inversion—instead of temperature increasing with depth and the regional geothermal gradient, the temperature in this borehole decreases with depth. This is likely because this well is surrounded by pavement that can store heat in the shallow subsurface. In the ambient temperature log, the temperature declines from 59.7 °F at the water level (62.5 ft) to 57.7 °F at about 205 ft below the measuring point. Below that, the temperature is constant, suggesting vertical flow. The FEC log over that range also suggests the possibility of ambient flow between the fractures at about 201.5 ft or 205 ft and the very bottom of the well, beyond where the OTV and ATV imaged.

HPFM data were collected above and below the fractures identified in the borehole image logs. There appeared to be possible minor upflow at the lower range of the HPFM tool from the bottom of the well to 214 ft. No upflow was measured in the borehole between 213 and 180 ft, which is consistent with the FEC log. However, upflow at the bottom of the borehole was minor. Under pumping conditions, all of the water captured with the HPFM was in the steel casing, indicating that the water came from the bottom of the casing. Because the borehole is slightly larger in diameter than the casing, there were concerns that the seal in the borehole was insufficient during flowmeter logging. Hence the HPFM was fit with larger size of flow diverter to improve the seal, and the logging was repeated. Both tests indicate that the highest amount of flow is at the base of casing. Observations made at the time of logging indicate water pumped from the well smelled like gasoline. In addition, the water was blackish and turbid. The turbidity cleared up a little, but the smell of gasoline continued during pumping.

Differencing the prepumping and postpumping FEC and TEMP logs (appendix 3, fig. 3–5) suggests that there is a change in the fluid water column coming from the zone at a depth of about 205 ft, where there is a fracture. The HPFM measurements indicated that under pumping conditions the only additional water came from the base of casing.

On July 30, 2014, 85–BR was pumped from the top of the borehole at a rate of 0.55 gal/min, which imposed a water-level decline of 2.4 ft. The flowmeter measurements were collected after the borehole reached quasi-steady state conditions after about 30 minutes of pumping. The specific capacity of the open borehole was 0.22 gal/min/ft of drawdown. By using

the methods of Bradbury and Rothschild (1985), the open-hole transmissivity was estimated at 45.8 ft^2/d. By using the methods of Srivastav and others (2007), the transmissivity was estimated at 21.6 ft^2/d.

FLASH was used to model zone head and transmissivity. Three zones were included in the model, including fractures (at midpoint depths of 203 and 230 ft) and at the base of casing at 141 ft. The flow measurements and the simulated flow profiles are shown in appendix 3 (fig. 3–6). A ROI of 100 ft was assumed, and the transmissivity was computed. The head and transmissivity of each fracture zone is listed in table 4. The total borehole transmissivity of 45.1 ft^2/d was estimated. The SSE was 2.4E-14 $(gal/min)^2$, which indicates a good fit of the simulated results compared to the observed flowmeter data. In this interpretation, 95 percent of the water was determined to come from the base of casing. In addition, fractures at a depth of 201 and (or) 205 ft bTOC contribute 2.5 percent to the transmissivity of the borehole, and the fracture at 230 ft bTOC accounts for 2.5 percent of the transmissivity.

Borehole radar.—In general, the directional and non-directional radar showed good depths of penetration, which is consistent with the resistive rock units surrounding the borehole. Analysis of the direct wave indicates the presence of lower velocity zones at depths of 145 to 148.2, 197.8 to 201.2 ft, and 212 to 222 ft below the measuring point. These zones appear to have clear reflectors in the radargram and some attenuation. One zone with a midpoint depth of about 159 ft shows a reflector with some attenuation but no clear reduction in velocity. At this depth in the OTV a felsic zone was identified, which would not be expected to produce a decrease in velocity, but a lithologic contact or felsic layer could cause a reflection consistent with what was observed in the data. The average velocity used to interpret the directional radar data was 390.1 ft/µs.

A total of seven reflectors were identified in the 60-MHz directional radar data. Two reflectors project outside the open section of the bedrock well. One reflector projects to intersect the borehole above the open hole and into the steel casing at a depth of 108 ft, and the other reflector is near the bottom of the borehole at 224 ft below the measuring point. Three reflectors appear to coincide with fractures identified in the ATV and OTV logs, including the transmissive zone at 141.4 ft (at the base of casing), the fracture at a depth of 212.6 ft, and the fracture at 219 ft below the measuring point. Two other reflectors appear to coincide with features that were identified in the image logs. The reflector at a depth of 159.1 ft coincides with a felsic layer in the borehole. The reflector orientation could only be resolved to ±180°. The other reflector at a depth of 196.2 ft coincides with foliation identified in the image logs. Interpretations of the radar logs are provided in a projection plot, a tadpole plot, and a stereoplot and in a table (appendix 3: fig. 3–7, fig. 3–8, table 3–2). In general, the radar reflectors for this borehole are similar in orientation to the fractures identified in the image logs. The one reflector that is clearly different is the steeply dipping reflector whose projection intersects the borehole at a depth of about 307 ft bTOC, which is below the bottom of the borehole.

Borehole 79/81–BR

Borehole location and construction.—The 79/81–BR borehole is a domestic well for the properties at 79/81 Bridge Road (fig. 1, table 1). It was initially a dug well. In 1977, a 6-inch-diameter well was drilled into the bedrock through the bottom of the dug well with cable-percussion drilling methods. The driller's yield was reportedly 4 gal/min at the time of drilling. Prior to the logging of 79/81–BR, gravel was added to the annular space around the steel casing and inside the 3-ft-diameter cement casing. Geophysical logs were collected in 79/81–BR from August 5, 2014, to August 7, 2014. The open-hole water level was 66.5 ft bTOC (table 1). Borehole and geophysical logging history are shown in appendix 4 (fig. 4–1). Geophysical logs and results are shown in appendix 4 (figs. 4–2 through 4–8, tables 4–1 and 4–2).

The well was completed to a total depth of 230 ft bTOC. All measurements were taken from the top of the 3-ft-diameter cement casing, which is about 1.3 ft above land surface. The cement casing is also about 5 ft above the 6-inch-diameter steel casing. The steel casing extends to a depth of 138 ft below the measuring point on the top of the cement casing. Borehole deviation logs in 79/81–BR indicate that the borehole deviates less than 1 ft and is essentially vertical (appendix 4, fig. 4–2).

Lithologic characterization.—Gamma, EMI, and ATV reflectivity (not shown) are fairly uniform (appendix 4, fig. 4–3). OTV logs show only small variations in the rock type. The OTV log shows that the formation from the bottom

Table 4. Hydrologic analysis of flow in borehole 85–BR, in the Tylerville study area, Haddam, Connecticut.

[Radius of investigation = 100 feet (ft). ft^2/d, foot squared per day; TOC, top of casing]

Depth of transmissive zone, in ft	Ambient flow above transmissive zone, in ft	Pumped flow above transmissive zone, in ft	Zone transmissivity, in ft^2/d	Depth to water level, in ft below TOC	Water level elevation, in ft	Percent of total transmissivity
141.00	0.00	0.61	42.9	62.23	7.77	95
203.00	0.00	0.03	2.2	62.23	7.77	5

of casing to a depth of about 180 ft is generally light in color with laminated banding. From a depth of about 180 to 210 ft the formation is darker, potentially because of more foliation and dark biotite (black, platy, foliated minerals). However, there are no other variations in the standard logs over this depth interval. Below the depth of 212 ft, the formation is characterized by more felsic bands and boudins. The stereoplots indicate that the poles to foliation planes and felsic layers cluster fairly tightly near the center of the stereoplot, indicating a shallow dip. The foliation is clustered and has an average orientation that strikes TN. 105° E. and dips 8° south-southeast. The nearly horizontal foliation is consistent with the lack of deviation in the borehole, as most wells typically deviate toward a direction normal to the foliation.

Fracture characterization.—The OTV and ATV images were interpreted together. The results are shown in the form of a projection plot, a tadpole plot, and a stereographic projection (appendix 4, fig. 4–4). The orientations of all fractures identified in the image logs are provided in tables and figures (appendix 4, fig. 4–4, table 4–1). Major fractures (in red, appendix 4, fig. 4–4) were identified in image logs. All of the major fractures were shallow in dip (less than 10°) with variable strikes (northwest, northeast, and southeast). The transmissive fractures were identified at depths of 143, 189, 206, and 220 ft bTOC. The orientations of these transmissive fractures average TN. 165° E., 10° (dipping to the southwest).

Hydraulic characterization.— Pumping of the nearby wells is likely to have interfered with the HPFM logging for this well. The ambient HPFM log collected on the evening of August 5, 2014, showed a few transient responses, which were consistent with the cycling on and off of nearby pumping. On August 6, 2014, the ambient as well as the pumping HPFM logs showed some transient responses to pumping in nearby wells; these responses were likely caused by the 3-gal/min sample pumping being conducted in 85–BR and 76–BR at that time. Cross-hole flowmeter tests were not used to quantify the hydraulics of the interconnections. However, the water level and HPFM data indicate cross-connections in the formation that could potentially be quantified with cross-hole flowmeter methods.

The FEC, TEMP, and SC logs collected before and after pumping suggest inflow to this well at depths of about 190, 206, and 220 ft, with possible minor inflow at 173 ft bTOC. The FEC, TEMP, and SC logs show strong stairstep anomalies, suggesting water of different specific conductance (appendix 4, fig. 4–5). The differencing log indicates that the fractures at about 190 ft and 206 ft bTOC contribute the water to the well under pumping conditions. The fractures at 220 and about 175 ft appear to have minor contributions to the fluid column.

HPFM logs collected on August 5 and 6, 2014, indicate the borehole had transient ambient flow in response to pumping from other wells. No constant ambient flow was observed. On August 6, 2014, when the borehole was pumped at 0.55 gal/min, the water levels reached steady-state conditions after about 20 minutes of pumping and declined a total of 13.85 ft. The specific capacity of the open borehole was 0.04 gal/min/ft of drawdown. By using the methods of Bradbury and Rothschild (1985), the open-hole transmissivity was estimated at 7.0 ft^2/d. By using the methods of Srivastav and others (2007), the transmissivity was estimated to be 2.3 ft^2/d.

Three of the inflow zones inferred in the fluid differencing logs were confirmed with the HPFM. Hydraulically active fractures were identified at 189 and 206 ft below the top of the cement casing. It also appears that there is a hydraulically active fracture or fractures near the top of the well around 140 to 143.5 ft. The inflow zone suggested by the change in the water column at about 175 ft could not be confirmed with the HPFM. The zone at 220 ft was included in the FLASH models because of the minor flow suggested in the fluid logs. The ambient and pumped HPFM data were simulated by using FLASH, and the total well transmissivity was 8.4 ft^2/d (appendix 4, fig. 4–6). The simulated results produced a solution that had an SSE that was 1.4 E-10 $(gal/min)^2$. Table 5 shows the amount of water yielded from each of the transmissive zones and the relative proportions of these amounts.

The measurements under ambient and pumping conditions and the simulated flow profiles are shown in appendix 4 (fig. 4–6). The flow profiles were modeled with three fractures, at depths of 189, 206, and 220 ft bTOC. In this model, the fractures centered at a depth of 189 ft account for 60 percent of the transmissivity of the well. The fracture at a depth of 206 ft accounts for 39 percent of the transmissivity, and the last 1 percent was attributed to the deepest fracture at a depth of 220 ft bTOC (table 5).

Table 5. Hydrologic analysis of flow in borehole 79/81–BR, in the Tylerville study area, Haddam, Connecticut.

[Radius of investigation = 100 feet (ft). ft^2/d, foot squared per day; TOC, top of casing]

Depth of transmissive zone, in ft	Ambient flow above transmissive zone, in ft	Pumped flow above transmissive zone, in ft	Zone transmissivity, in ft^2/d	Depth to water level, in ft below TOC	Water level elevation, in ft	Percent of total transmissivity
189.00	0.00	0.62	5.0	71.28	2.22	60
206.00	0.00	0.25	3.3	71.28	2.22	39
220.00	0.00	0.01	0.1	71.28	2.22	1

Borehole radar.—Analysis of the 250-MHz nondirectional dipole radar surveys indicates low-velocity zones at depths of 141 to 143 (near casing), 172 to 178, 188 to 190, and 205 to 213 ft bTOC (appendix 4, fig. 4–7). Each of these zones is associated with reflectors in the radar image. Only two of the reflectors, which are centered on depths of 142 and 175 ft, have an increase in attenuation along with the decrease in velocity, characteristic of water-filled fractures. However, two of the other zones (at depths of 189 and 206 ft bTOC) were identified as transmissive. Another very strong reflector projected to the bottom of the borehole and is likely the feature identified in the directional radar data at the depth of 233.9 ft bTOC.

A total of eight reflectors were interpreted from the directional borehole-radar reflection survey conducted in 79/81–BR. One reflector was projected to intersect the borehole behind casing at a depth of about 119 ft. The strike and dip of this feature is TN. 16° E., 20° (dipping southeast). Three reflectors project to intercept below the bottom of the borehole at depths of about 244, 258, and 302 ft bTOC. These features vary in orientation—there is one horizontal feature at a depth of 244 ft and two moderately dipping features with strikes to the north (TN. 356° E.) and to the south (TN. 196° E.). Another very strong reflector, which intersects the borehole at a depth of 233.9 ft, is at the very bottom of the open borehole and beyond the depth of the imaging tools. This strong reflector has an orientation of TN. 336° E., 38° E. and is approximately parallel to the feature at a depth of 258 ft bTOC. Three of the other features correlate in depth and orientation with features in the image logs. The reflector at a depth of 141.7 ft coincides with a northwest strike, shallow dip (TN. 337° E., 19° E.) feature. The strong reflector (with a high confidence in orientation) at a depth of 217.5 ft (near the depth of the low-radar-velocity zone at 220 ft) coincides with a transmissive fracture with a south-southeast strike and shallow dip (TN. 165° E., 10° E.). A comparison of the stereoplots for the image logs (appendix 4, fig. 4–4) and the radar stereoplot (appendix 4, fig. 4–8) shows that the radar images more steeply dipping features than what can be seen in the boreholes alone. All radar information for 79/81–BR is summarized in appendix 4 (figs. 4–7 and 4–8, table 4–2).

Borehole 77–LMR

Borehole location and construction.—Domestic well 77–LMR at 77 Little Meadow Road was drilled in 1985 by air-rotary drilling methods (fig. 1, table 1). The well driller's yield was estimated at 5 gal/min at the time of drilling. The steel casing extends from 0.82 ft above land surface to a total of 155.5 ft bTOC. The well was completed to a total depth of 343.75 ft bTOC. Geophysical logs were collected in 77–LMR on June 26–27, 2014. All depths were referenced to the top of casing. Borehole and geophysical logging history is shown in appendix 5, fig. 5–1. Borehole logs, plots, and tables are provided in appendix 5 (figs. 5–2 through 5–8, tables 5–1 and 5–2). Borehole deviation logs indicate 77–LMR is nearly vertical. The well deviates a total of 2.5 ft over the 340-ft depth toward the southwest (appendix 5, fig. 5–2).

A small piece of tubing with a metal ferule can be seen in the OTV, ATV, and EMI logs near the bottom of the well from a depth of 310 to 340 ft. The tubing and fitting appear to be part of the water-supply system. Borehole tools were able to pass by the tubing, and it did not impede access to the bottom of the well. The tubing could not be removed with one of the tools. The ambient water level was 5.47 ft bTOC on June 26, 2014. The water level in 77–LMR appears to vary with tidal fluctuations—about 2.19 ft over a daily cycle.

Lithologic characterization.—Borehole imaging logs and conventional logs indicate the rock type is a banded gneiss (appendix 5, fig. 5–3). The driller's log indicates the driller encountered bedrock at a depth of 139 ft, which is consistent with the small increase in natural gamma counts at that depth through the steel casing. From the bottom of casing at 155.5 ft to depths of about 200 ft, the rock appears to be dark with narrow banding. From depths of about 200 to 300 ft, the rock has more felsic banding than at the top of the well. Large felsic zones are observed in the OTV log at depths of 212 to 221 ft, 246 to 249 ft, and 254 to 260 ft bTOC. The felsic zones in 77–LMR dip gently to the east. The bottom of the borehole is characterized by dark foliated rock with some felsic banding and boudins. The stereoplots indicate the foliation and banding is generally shallow dipping. The average orientation of foliation strikes TN. 159° E. and dips gently (14° to the east).

Fracture characterization.—The OTV and ATV images were interpreted together. The results are shown in the form of a projection plot, a tadpole plot, and a stereographic projection (appendix 5, fig. 5–4). The orientations of all fractures identified in the image logs are provided in tables and figures (appendix 5, fig. 5–4, table 5–1). Fractures are generally parallel to the foliation and fabric of the bedrock. The transmissive zones were at identified at depths of 156 ft bTOC at the base of casing and at fractures at 193, 307, and 331 ft bTOC. The orientations of these transmissive fractures are in two clusters. One cluster, which is nearly parallel to foliation, strikes southeast and dips gently to the southwest. The other cluster strikes to the north and dips to the east.

Hydraulic characterization.—The FEC, TEMP, and SC logs collected before and after pumping suggest that there is inflow to this well at depths of about 156 ft near the base of casing and 193 ft bTOC (appendix 5, fig. 5–5). The differences in these water properties in the fluid in the borehole may indicate the zone where the flow associated with the change in borehole storage enters and exits the well. Under close inspection of the differences in the logs from before and after pumping, there appear to be contributions to the well from depths of 156, 193, 307, and 331 ft bTOC. Each of these inflow zones was confirmed with the HPFM.

HPFM logs collected on June 26, 2014, indicate the borehole had ambient flow that was associated with a change in borehole storage. The water level in the borehole goes up and down with the stage in the river, and the water flows in and out

of specific fractures. When the flow rate was corrected for the changes in borehole storage, there was no ambient flow (from one fracture to another). Table 6 shows the amount of the water yielded from each of the transmissive zones and their relative proportions.

On June 26, 2014, 77–LMR was pumped at 0.5 gal/min, for 2 hours. The water level reached steady-state conditions after 11 minutes of pumping, and it only declined a total of 0.25 ft. The specific capacity of the open borehole was 2.0 gal/min/ft of drawdown. By using the methods of Bradbury and Rothschild (1985), the open-hole transmissivity was estimated at 470 ft^2/d. By using the methods of Srivastav and others (2007), the transmissivity was estimated at 372.5 ft^2/d.

The ambient and pumped flow profiles were simulated by using FLASH. The total transmissivity was estimated at 367 ft^2/d with a ROI of 100 ft (appendix 5, fig. 5–6). 77–LMR is the most transmissive borehole in the investigation. The most transmissive zone is at the bottom of the well at a depth of 331 ft. It accounts for 40 percent of the total transmissivity. The fracture at 307 ft accounts for 30 percent of the transmissivity in the borehole. The fractures at depths of 193 and 156 ft bTOC account for 14 and 16 percent, respectively. The simulated results produced solutions that had an SSE that was 2E-13 $(gal/min)^2$.

Borehole radar.—Analysis of the direct wave indicates zones of slightly lower velocity at center depths of 193, 240, 288, 305, and 320 ft bTOC. These zones appear to have clear reflectors. One low-velocity zone was identified from depths of 188.7 to 198.4 ft bTOC and had increased attenuation at this depth. The radar reflections at this depth are subtle but clear. This zone coincides with a zone that was determined to be transmissive. The hint of another low-velocity zone was identified near the base of casing at a depth of 158 ft bTOC and coincides with a transmissive fracture.

One clear reflector that appears to project to the well at about 230 ft bTOC shows only a weak or slight decrease in velocity from a depth of 225 to 249 ft bTOC (appendix 5, fig. 5–7). The transmissive zone at 307 ft shows a minor decrease in velocity and increase in dielectric permittivity but no associated increase in attenuation. The transmissive zone at 330 ft may have reflectors associated with it, but there is no clear decrease in the velocity.

The 60-MHz directional radar data showed good depths of penetration, which is consistent with the resistive rock units surrounding the borehole. A total of 16 reflectors were identified in the 60-MHz directional radar data. Five reflectors project to outside the open section of the bedrock well. One reflector projects to intersect the borehole above the steel casing at a depth of 137.1 ft. The other reflectors project below the bottom of the borehole at depths of 373, 418, 419, and 432 ft bTOC. Nine reflectors appear to coincide with features identified with the image logs, including the transmissive zones at 167, 183, and 332 ft bTOC. Two other reflectors appear to coincide with features that were identified in the image logs at depths of 273 and 240.5 ft bTOC. The reflector at a depth of 268.1 ft coincides with a felsic layer in the borehole. The other two reflectors at depths of 301 and 317 ft coincide with foliations identified in the image logs. Interpretations of the radar logs are provided in a projection plot, a tadpole plot, a stereoplot, and in a table (appendix 5: fig. 5–7, fig. 5–8, table 5–2).

Borehole 130–LMR

Borehole location and construction.—130–LMR is located near the banks of the Connecticut River at 130 Little Meadow Road (fig. 1, table 1). The well was drilled on October 16, 1991, to a depth of 345 ft below land surface for use as a domestic water supply. Drilling logs indicate the bedrock surface was 99 ft below land surface. Geophysical logs were collected from June 24 to 25, 2014. All depth measurements were referenced to the top of steel casing, which is 2.33 ft above the land surface. Borehole and geophysical logging history are shown in appendix 6 (fig. 6–1). Geophysical logs and results are shown in appendix 6 (figs. 6–2 through 6–8, tables 6–1 and 6–2).

The steel casing extends to a total depth of 108.5 ft below top of casing. The borehole deviates a total of 8.5 ft (off center) toward the northeast with most of the deviation occurring from the bottom of casing to the bottom of the borehole (108 to 345 ft below top of casing). The water level on June 24, 2014 at 6:10 PM was about 6.65 ft below the top of casing. The open-hole water levels appear to vary with tidal fluctuations—about 1.8 ft over a daily cycle.

Table 6. Hydrologic analysis of flow in borehole 77–LMR, in the Tylerville study area, Haddam, Connecticut.

[Radius of investigation = 100 feet (ft). ft^2/d, foot squared per day; TOC, top of casing]

Depth of transmissive zone, in ft	Ambient flow above transmissive zone, in ft	Pumped flow above transmissive zone, in ft	Zone transmissivity, in ft^2/d	Depth to water level, in ft below TOC	Water level elevation, in ft	Percent of total transmissivity
156.00	0.00	0.50	51.4	5.75	2.07	14
193.00	0.00	0.43	56.7	5.75	2.07	16
307.00	0.00	0.35	110.1	5.75	2.07	30
331.00	0.00	0.20	146.89	5.75	2.07	40

Lithologic characterization.—Borehole imaging logs and conventional logs indicate the rock type is a banded gneiss (appendix 6, fig. 6–3). The OTV log provided high-quality images of the gneiss. In the OTV log the rock type is characterized with dark-gray layers with schistose zones and equigranular, fine-medium grained, greenish-gray zones that are interpreted as calc-silicate layers. Felsic layers, which are visible in the OTV log by t a lighter rock color than the adjacent zones, were observed at depths of 110 to 114.5 ft, 128 to 131 ft, and 141 to 144 ft, and a narrow band was observed at 168 ft. The calc-silicate is massive and greenish gray in color, from 198 to 215 ft bTOC. The stereoplots indicate the poles to foliation planes, and felsic layers cluster near the center of the stereoplot, indicating a shallow dip. In general, the foliation strikes TN. 157° E. and dips at a shallow angle (11°) to the southwest. The image log shows that there are felsic lenses and boudins below 216 ft to the bottom of the borehole.

Fracture characterization.—The OTV and ATV images were interpreted together. The results are shown in the form of a projection plot, a tadpole plot, and a stereographic projection (appendix 6, fig. 6–4). Two sets of major fractures were identified with the image logs. One set is parallel to the foliation and fabric of the bedrock. The other set has an average strike of TN. 71° E. and an average dip of 66° toward the northeast. The transmissive fractures were identified at depths of 108.5, 232, and 260 ft bTOC. The orientations of these transmissive fractures have an average strike of TN. 234° E. and dip gently (13°) to the southwest.

Hydraulic characterization.—HPFM logs collected on June 25, 2014, indicate the borehole had minor ambient flow (appendix 6, fig. 6–5). Under pumping conditions of 0.6 gal/min, the water levels reached steady-state conditions after 6 minutes of pumping and declined a total of 0.58 ft. The specific capacity of the open borehole was 1.05 gal/min/ft of drawdown. By using the methods of Bradbury and Rothschild (1985), the open-hole transmissivity was estimated at 235 ft^2/d. By using the methods of Srivastav and others (2007), the transmissivity was estimated at 161.5 ft^2/d.

There was a minor amount of water coming out of the bottom of casing at a depth of 108.5 ft bTOC. During the time of logging, the water flowed vertically through the borehole and exited at the fracture at a depth of 260 ft bTOC. The measured ambient downflow rate was reduced by the rate of change in borehole storage, which was caused by the effect of tidal fluctuations on the water level. Under steady-state pumping conditions, most of the water came from the bottom of casing. In addition, water entered the borehole from the fractures at depths of 232 and 260 ft bTOC. The OTV log showed a feature at a depth of about 305 ft with a dark vertical line, which may represent some sort of precipitate, on one side of the borehole. Initial field data suggested possible minor flow from a fracture from 300 to 305 ft, but this could not be modeled in FLASH. The upward flow was less than the resolution of the flowmeter (appendix 6, fig. 6–5).

The ambient and pumped flow profiles were simulated by using FLASH. The total transmissivity of the borehole was estimated to be 233 ft^2/d with a ROI of 100 ft (appendix 6, fig. 6–6). The simulated results produced a solution that had a SSE that was about 2.4E-9 $(gal/min)^2$. The head and transmissivity of each fracture zone is listed in table 7. In this model, the uppermost zone accounted for 58 percent of the total transmissivity of the borehole. The other two fractures at 232 and 260 ft accounted for 19 and 23 percent of the transmissivity, respectively.

Borehole radar.—Analysis of the 250-MHz nondirectional dipole radar surveys indicate low-velocity zones at 117 to 123.4, 186.4 to 198.4, 222 to 232, 285.9 to 296.2, and 327 ft bTOC. These low-velocity zones were characterized with strong reflectors in the radargram. These zones were also characterized with relatively high attenuation. The average velocity used to interpret the directional radar data was 391.8 ft/µs.

A total of 18 reflectors were interpreted in the radar reflection survey. One reflector projects to the well depth at -55.4 ft above the top of casing, and has an average strike of TN. 126° E., with a moderate dip (55°) to the southwest. Four other reflectors project to above the open section of the borehole to intersect the borehole at depths of about 46, 59, 67, and 92 ft above the top of casing. These features, if continuous, intersect the bedrock surface at a distance from the well. Four reflectors project to below the borehole, and two reflectors project to near the bottom of the well, below where the full length of the radar tool can fit. These features were observed in the formation surrounding the well and project to intersection depths of about 317, 342, 357, 402, 418, and 490 ft bTOC. Their quality scores indicate they are fairly continuous, but their orientations have fairly high uncertainty.

Table 7. Hydrologic analysis of flow in borehole 130–LMR, in the Tylerville study area, Haddam, Connecticut.

[Radius of investigation = 100 feet (ft). ft^2/d, foot squared per day; TOC, top of casing]

Depth of transmissive zone, in ft	Ambient flow above transmissive zone, in ft	Pumped flow above transmissive zone, in ft	Zone transmissivity, in ft^2/d	Depth to water level, in ft below TOC	Water level elevation, in ft	Percent of total transmissivity
108.00	0.00	0.61	134.6	5.60	0.74	58
232.00	-0.02	0.24	44.0	5.58	0.72	19
260.00	-0.02	0.13	54.6	5.52	0.66	23

These reflectors that project to below the borehole are steeply dipping. Six reflectors coincide with foliations observed in the image logs. Three reflectors coincide with major fractures, and one reflector coincides with a transmissive fracture (at a depth of 232 ft). Ten reflectors that project to the open hole do not coincide with OTV features and were "radar only" features (appendix 6, fig. 6–7, table 6–1). Stereoplots for the radar features show that the radar imaged more steeply dipping features than the imaging tools sampled in the boreholes.

Eight reflectors coincide with the orientation of features observed in the borehole. These features generally strike TN. 155°E. and have shallow to moderate dips to the southwest. The reflector at 232 ft is coincident with the transmissive fracture identified in the borehole and within one of the low-velocity zones identified in the nondirectional dipole data. The locations and orientations of reflectors are shown in a projection plot, a tadpole plot, and a stereoplot. All radar information for 130–LMR is summarized in appendix 6 (figs. 6–7 and 6–8, table 6–2).

Borehole 95–BR

Borehole location and construction.—95–BR is located at 95 Bridge Road (fig. 1, table 1). 95–BR is a monitoring well that was formerly used as a production well for the manufacturing facility that formerly operated at this address. Little is known about the well's construction and completion. Although no well-completion report exists, the well was reportedly drilled to a total depth of 330 ft. However, a rubber cylindrical gland (approximately 2 ft long) had been extended on a pipe to a depth of about 136 ft bTOC. The pipe and rubber gland, as well as other debris were removed from the well in July 2014. The well was logged August 1, 2014. All measurements were referenced to the top of casing, which is at land surface. Borehole and geophysical logging history are shown in appendix 7 (fig. 7–1). Geophysical logs and results are shown in appendix 7 (fig. 7–2).

The complete depth of the well is at least 308 ft bTOC, as determined with a steel tape. The tape got caught at several places while sounding the well, which is consistent with possible constrictions or obstructions in the well. The water level was 66.5 ft bTOC.

The fluid conductivity and temperature were collected on the passage down the well. The tool was lowered to a total depth of 308 ft below land surface, and caliper data were collected as the tool came up the borehole. There were constrictions from depths of 78 to 87 ft, 132 to 142 ft, and 300 to 307 ft bTOC. At a depth of 89.9 ft, the constriction was less than 3 inches in diameter. These constrictions prevented the smooth passage of the tool. At the constriction at a depth of 142 ft, the caliper tool had to be closed and pulled through the constricted section, and caliper data were not collected from about depths of about 139 to 135 ft bTOC. The caliper log identified fractures at depths of at depths of 282 ft below land surface. Geophysical logs and results are shown in appendix 7 (fig. 7–2).

Fracture characterization.—The casing is 8 inches in diameter, and it appears that the bottom of casing is either at about 78 or 130 ft below land surface, based on the smoothness of the caliper log. The caliper log shows some minor enlargements that suggest the presence of fractures at depths of about 95, 148, 167, 183, and 231 ft below land surface. There appear to be changes in the fluid conductivity and temperature at the enlargements at 148, 182, and 231 ft bTOC.

Because of the constrictions in the borehole, no other logs were run in the borehole. However, a video camera was used to help determine what the obstructions were. Images were inconclusive; the deepest depth attained was about 80 ft.

Combined Results From All Wells

Borehole imaging logs and conventional logs from the six boreholes indicate the rock type is a banded gneiss. This is consistent with the Hebron Gneiss, which has been mapped in this area in local and regional maps. The OTV logs provided high-quality and clear images of the gneiss. The rock is characterized with dark-gray layers with schistose zones and equigranular, fine-medium grained, greenish-gray zones that are interpreted as calc-silicate layers. Felsic layers characterized by a lighter rock color than adjacent zones were observed in the OTV images in each of the wells.

Projection plots, tadpole plots, and stereoplots were generated for each borehole so that the orientations of foliation, fractures, and reflectors could be observed with location, depth, and rock type (appendixes 1–6). In addition, stereoplots were generated for each of the six boreholes and for the combined results from all the boreholes (figs. 8*A–D*). Figure 8 offers a means to assess changes in orientation of these features over the study area. The orientation of the fabric (foliation and layering in the banded gneiss) is fairly constant across the study area. The stereoplots for foliation (fig. 8*A*) show a fairly tight clustering of poles to planes in each of the boreholes. The foliation dips gently to the south-southwest, with an average strike and dip of TN. 152° E., 11° SW. The fractures observed in the six logged boreholes have poles to fracture planes in the stereoplots that are generally in two clusters (fig. 8*B*). One cluster coincides with the foliation of the rock. The second, weakly clustered set dips gently to the northeast with an average strike of TN. 334° E., dipping 50° northeast. The poles to planes of the radar reflectors (fig. 8*C*) show a strong clustering of poles that coincide with the foliation-parallel fractures. In addition, there are numerous reflectors that are more steeply dipping than the features in the boreholes. These features strike in various directions. In all of the wells, except 79/81–BR, there are steep, east-striking, south-dipping reflectors. In each of 1640–SR, 77–LMR, and 130–LMR, there is a small cluster of north-northwest-striking and east-northeast-dipping reflectors. Only 130–LMR has a small cluster of poles to planes that are southwest striking and northwest dipping.

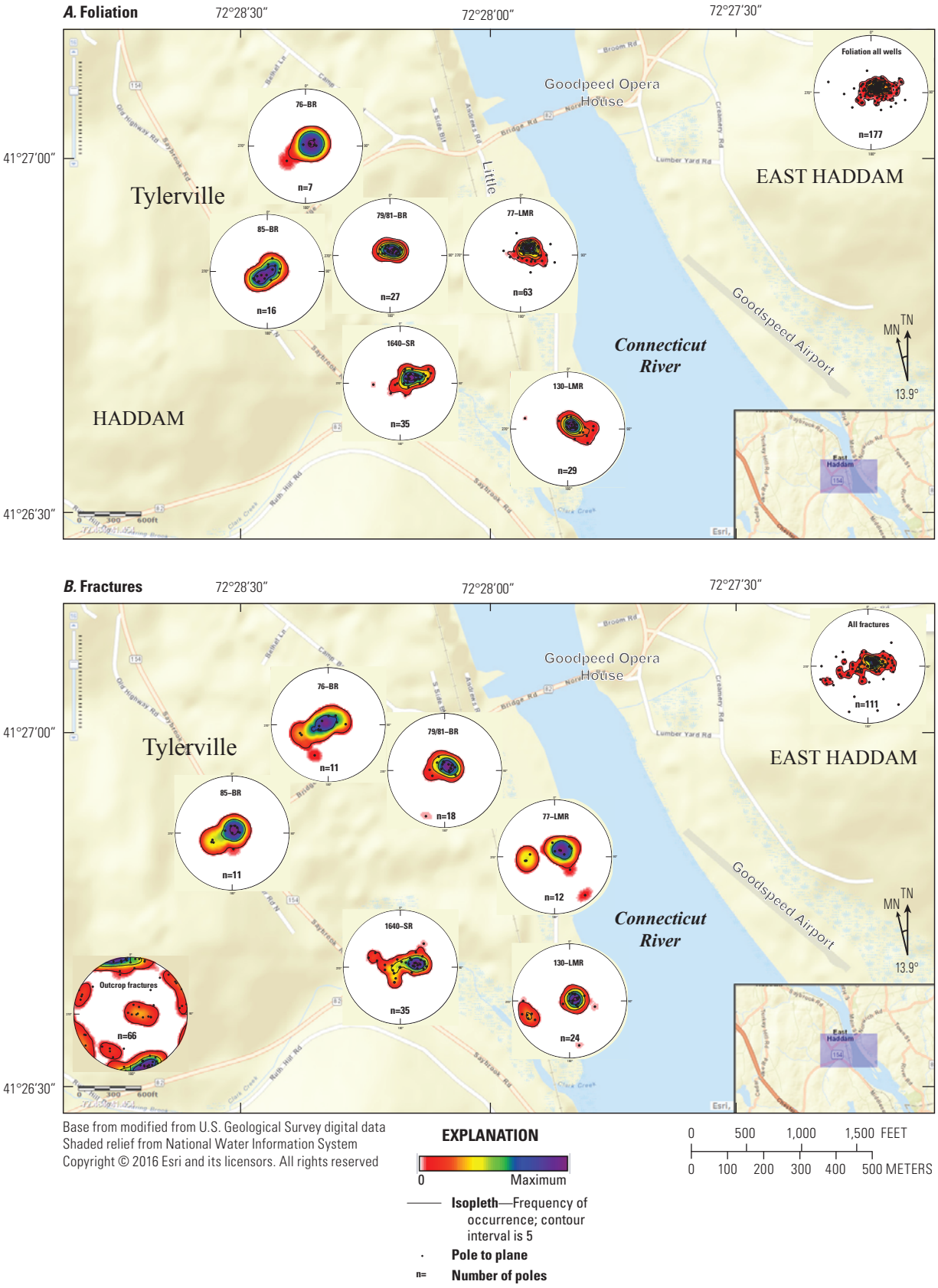

Figure 8. Stereoplots of *A*, foliation measured from televiewer logs; *B*, fractures measured from televiewer logs; *C*, reflectors interpreted from borehole radar logs and *D*, fractures and borehole-radar reflectors, with a Terzaghi (1965) correction applied, for boreholes in the Tylerville study area, Haddam, Connecticut, 2014. The outcrop fractures include measurements made by Loureiro Engineering Associates, Inc., and by the Connecticut Department of Energy and Environmental Protection. MN, magnetic north; TN, true north.

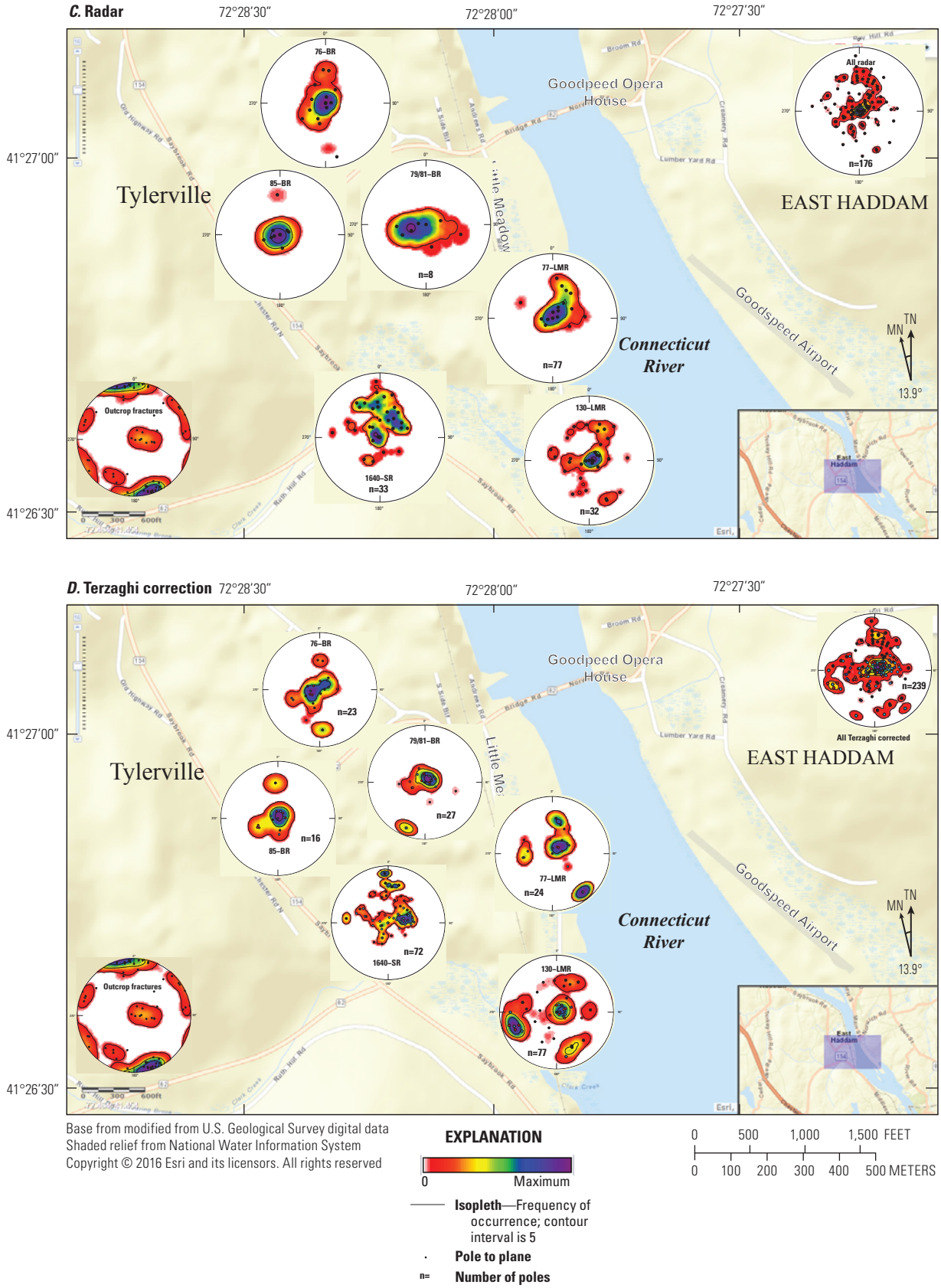

Figure 8. Stereoplots of *A*, foliation measured from televiewer logs; *B*, fractures measured from televiewer logs; *C*, reflectors interpreted from borehole radar logs and *D*, fractures and borehole-radar reflectors, with a Terzaghi (1965) correction applied, for boreholes in the Tylerville study area, Haddam, Connecticut, 2014. The outcrop fractures include measurements made by Loureiro Engineering Associates, Inc., and by the Connecticut Department of Energy and Environmental Protection. MN, magnetic north; TN, true north.—Continued

Fracture data from the outcrop mapping, collected as part of the supplemental fracture investigation by the CT DEEP and Loureiro Engineering Associates, Inc., was included on the western side of figure 8 ("Outcrop fractures"). The relative proportions of steep and shallow fractures in the outcrop stereoplot highlight the sampling bias of fractures observed in boreholes relative to fractures observed in outcrop. Outcrops tend to "sample" more steeply dipping features than boreholes. Most boreholes and wells drilled for water supply are nearly vertical and, therefore, are less likely to intersect steeply dipping features. Because vertical boreholes statistically undersample steeply dipping features, a sampling bias correction is often applied (Terzaghi, 1965) to expand a biased dataset that undersamples vertical features to include more steeply dipping fractures.

The fact that the fracture sets from the borehole imaging have so few steeply dipping fractures indicates the Terzaghi correction would not increase the population of the steeply dipping fractures by much (as the correction attempts to reapportion the number of steeply dipping fractures observed in the borehole). Therefore, a new dataset was generated from the combination of the fractures observed in the imaging logs and radar reflectors, which sample more steeply dipping features. Care was taken to not duplicate the fractures seen in both methods. After the Terzaghi correction was applied to the combined dataset, the population of the steeply dipping fractures greatly increased (fig. 8*D*). If fractures from a larger area (such as what is sampled with the radar) were included in the dataset, then the Terzaghi correction would likely overestimate the number of steeply dipping fractures in the population at that well location. However, the resultant stereoplot would appear more like stereoplots from outcrops and should be viewed conceptually. In figure 8*D*, the Terzaghi-corrected stereoplots look more like the actual outcrop map; however, they do not show the strong clusters of nearly vertical, west-east trending, and north-south-dipping fractures that were observed in the outcrop stereoplots.

The hydraulic characterization of the boreholes included differencing of the FEC, TEMP, and SC logs collected before and after pumping along with the HPFM profiles to identify transmissive fractures. In several cases, the fluid-differencing log helped interpretations of the flowmeter data. Under low-rate pumping conditions of about 0.5 gal/min, two to four fractures were identified in each well. Flowmeter data that were processed in FLASH produced open-hole and discrete-interval values for the transmissivity and head.

The transmissivity estimates for open-hole, total well transmissivity based on FLASH ranged from 4.9 to 367 ft^2/d, for an ROI of 100 ft. Reducing the ROI to 50 ft only reduced the transmissivity estimates to range from 4.3 to 324 ft^2/d (table 8). The FLASH transmissivity estimates were similar to the estimates made by using the method of Bradbury and Rothschild (1985), which ranged from 3.2 to 470 ft^2/d. The estimates of transmissivity made by using specific capacity and an empirical equation of Srivastav and others (2007) ranged from 1.0 to 372 ft^2/d; they were lower than estimates made through the other two approaches but were well within an order of magnitude. The open-hole transmissivity values estimated for wells in this investigation are summarized in table 8. In general, the open-hole transmissivity estimates show fairly good correlation between the transmissivities determined with the three methods. The HPFM analysis was able to apportion the transmissivity to the most transmissive fractures identified in the borehole within the dynamic resolution and measurement resolution of the HPFM. These methods produce consistent results that are all within an order-of-magnitude estimate.

The boreholes in this investigation had 11 to 35 fractures observed in each borehole image, but each borehole had only 2 to 4 fractures with transmissivity large enough to measure with flowmeter methods. In this investigation, the transmissivity of the individual fracture zones, as identified by using a heat-pulse flowmeter, varied over three orders of magnitude and ranged from 0.1 to 130 ft^2/d. However, the actual fracture

Table 8. Results of transmissivity calculations, using different methods, for wells in the Tylerville study area, Haddam, Connecticut.

[ROI, radius of influence; ft, feet; (gal/min)/ft, gallon per minute per foot]

Well name	Transmissivity, in feet squared per day, by method of calculation				Specific capacity, in (gal/min)/ft
	Heat-pulse flowmeter, ROI = 50 ft	Heat-pulse flowmeter, ROI = 100 ft	Bradbury and Rothschild (1985), full time of pumping, for an open hole	Srivastava and others (2007) method using specific capacity	
1640–SR	17.5	19.8	20.5	8.6	0.11
76–BR	4.3	4.9	3.2	1.0	0.02
85–BR	39.9	45.1	45.8	21.6	0.22
79/81–BR	7.4	8.4	7.0	2.3	0.04
77–LMR	324	367	469.7	372.5	2.00
130–LMR	206	233	234.6	161.5	1.05

transmissivity in crystalline rock varies over 10 orders of magnitude (Shapiro, 2001). This difference in orders of magnitude underscores the point that the methods used in this investigation identify the most transmissive fractures in the boreholes, but they do not identify all of the transmissive fractures. This observation leads to a conceptual model in which highly transmissive fractures, whose transmissivity can be measured with flowmeter methods, are embedded within a network of less transmissive fractures.

The borehole geophysical data from this site indicate moderate fracturing, with numerous and variable fracture orientations in the near surface and over the depths intersected by the boreholes. The conceptual model is that the fractures form a three-dimensional network of blocks and fractures that act at some scale as a continuum. In general, water flows from recharge areas toward discharge areas, and regional groundwater flow is inferred to follow land-surface topography with downward movement in recharge locations and upward flow in discharge locations. Locally, the direction of groundwater flow is affected by small-scale topographic features, directions of fractures relative to the hydraulic gradient, effects of pumping, and, in some cases, tidal influences. The actual flowpaths that water and (or) contaminants follow can differ from the inferred regional flow. In this investigation, upflow was observed in 130–LMR near the river, and in 1640–SR near the wetland. Ambient flow associated with nearby pumping was observed in 76–BR, 85–BR, and 79/81–BR. These observations are consistent with the expected regional flow system and with the expected transient response of local well interference. To expand the conceptual groundwater-flow model for the site to describe contaminant flow, the data in this report would have to be coupled with geologic, hydrologic, and geochemical data to refine the conceptual flow model and determine contaminant pathways (Shapiro and others, 1999).

The data and interpretation presented in this report provide information that site investigators can use in planning and implementing sampling efforts and in refining the conceptual groundwater-flow model for the site. The geologic framework, fracture characterization, and estimates of hydraulic properties can be interpreted together to characterize the fracture network. Collectively, the results and the conceptual site model are important for evaluating contaminant distribution, for potential remediation options, and for planning borehole completions or borehole networks that will be adequate for monitoring flow, remediation efforts, groundwater levels, and (or) water quality.

Summary and Conclusions

During June to August 2014, the U.S. Geological Survey, in cooperation with the Connecticut Department of Energy and Environmental Protection, collected geophysical logs in seven active or former bedrock water-supply wells at a site in the Connecticut River Valley in the Tylerville section of Haddam, Connecticut. The purpose of the logging was to (1) identify and (or) validate well construction, (2) determine the rock type and orientation of the foliation and layering of the rock, (3) characterize the depth and orientation of fractures, (4) evaluate fluid properties of the water in the well, and (5) determine the relative transmissivity and head of discrete fractures. The digital data are provided with the report.

Residential, light industrial, and commercial properties in Tylerville rely on private wells for water supply. Many of these wells are completed in the bedrock. In the study area, gneissic bedrock is overlain by unconsolidated sediments consisting of alluvium, stratified drift, and ice-contact deposits ranging in thickness from about 1 to 200 feet. Previous investigations by the Connecticut Department of Energy and Environmental Protection indicated that contamination with chlorinated solvents and 1,4-dioxane is present in both the overburden and in the crystalline bedrock aquifers. In addition, methyl *tert*-butyl ether (MTBE) has been observed in water samples collected from other supply wells. These observations prompted further investigation of the overburden and fractured-rock aquifers by the Connecticut Department of Energy and Environmental Protection.

From June to August 2014, a full suite of geophysical logs were collected in six of the boreholes. These logs include caliper, formation conductivity and resistivity, natural gamma, optical and acoustic imaging, borehole deviation and tilt, temperature and fluid conductivity, single-hole flowmeter under ambient and stressed (pumping) conditions, and borehole radar. Collectively the logs were used to characterize the subsurface lithology, rock fabric (foliation and layering), and depth and orientation of fractures. In addition, the flowmeter logs were used to determine transmissivity and hydraulic head of the most transmissive fractures that intersect the borehole. A seventh borehole was to be logged with the full suite of tools; however, because of obstructions in the borehole, it was only possible to collect the fluid conductivity, temperature, and caliper logs in the borehole.

The orientation of the fabric of the rock varies but generally dips gently to the south-southwest. The fractures observed in the six logged boreholes cluster in two sets. Most of the fractures are parallel to the foliation. The second, weakly clustered set dips gently to the northeast. Because of the resistivity of the rock types, the radar was able to see tens of feet into the formation around the boreholes to image reflectors, which are caused by fractures or planar features in the rock. Because radar samples a larger volume of the subsurface, it is able to see more steeply dipping features than are seen in the borehole imaging data. The radar identified many reflectors that coincide with fractures in the borehole and are parallel to the foliation. In addition, the radar identified moderately to steeply dipping features that strike roughly east-west and dip to the south and north.

Flowmeter and fluid geophysical log data collected under ambient and pumping conditions were processed in Flow-Log Analysis of Single Holes (FLASH), a multilayer, Thiem-based analytical solution for steady-state flow in a single borehole,

to estimate discrete-interval and open-hole transmissivity and head. The discrete-zone transmissivity estimates provide quantified information on the sources of water to a given open-hole sample, which is typical of a sample collected from a domestic water system. The transmissivities of the boreholes ranged from 4 to 367 feet squared per day. These values are consistent with the transmissivity estimated from open-hole hydraulic tests that use the drawdown (specific capacity) and pumping rate, and ranged from 1 to 470 feet squared per day. These methods of testing produce consistent results that are all within an order-of-magnitude estimate.

The wells in this investigation are typical for wells in fractured crystalline rock, where wells typically have tens of fractures but only two or three fractures with transmissivity large enough to be measured with a flowmeter. In this investigation, the measured transmissivity of the individual fracture zones varied over three orders of magnitude from 0.1 to 130 feet squared per day. The actual fracture transmissivity in crystalline rock varies over ten orders of magnitude. This difference between measured and actual variation in transmissivity underscores the point that the methods used in this investigation identify the most transmissive fractures in the boreholes, but not all of the transmissive fractures, and leads to a conceptual model of highly transmissive fractures embedded within a network of less transmissive fractures.

The data and interpretation presented in this report provide information that can be used by site investigators for planning and implementing sampling efforts and for refining the conceptual model of groundwater flow at the site. The geologic framework, fracture characterization, and estimates of hydraulic properties can be interpreted together to characterize the fracture network. Collectively, the results and the conceptual site model are important for evaluating contaminant distribution, for potential remediation options, and planning borehole completions or borehole networks that will be adequate for monitoring flow, remediation efforts, groundwater levels, and (or) water quality.

References Cited

AECOM, 2010, Modified Phase I Environmental Site Assessment and Review of Historical Data Report for Tylerville Center, Final September 2010: AECOM report, publically available from Connecticut Department of Energy and Environmental Protection.

American Society for Testing and Materials, 2004, Standard D6167–97—Standard guide for conducting borehole geophysical logging—Mechanical caliper: West Conshohocken, Pa., American Society for Testing and Materials, 6 p.

American Society for Testing and Materials, 2001, Standard D7626–01—Standard guide for conducting borehole geophysical logging—Electromagnetic induction: West Conshocken, Pa., American Society for Testing and Materials, 7 p.

Bradbury, K.R., and Rothschild, E.R., 1985, A computerized technique for estimating hydraulic conductivity of aquifers from specific capacity data: Ground Water, v. 23, no. 2, p. 240–245.

Buursink, M.L., Lane, J.W., Jr., Clement, W.P., and Knoll, M.D., 2002, Use of vertical-radar profiling to estimate porosity at two New England sites and comparison with neutron log porosity, *in* Proceedings of the Symposium on the Application of Geophysics to Engineering and Environmental Problems, Las Vegas, Nevada, February 10–14, 2002, Proceedings: Denver, Colo., Environmental and Engineering Geophysical Society, CD–ROM, 12 p.

Connecticut Department of Energy and Environmental Protection, 2015, State of Connecticut Superfund Priority List: Connecticut Department of Energy and Environmental Protection, accessed June 21, 2016, at http://www.ct.gov/deep/cwp/view.asp?A=2715&Q=325020#Tylerville.

Day-Lewis, F.D., Johnson, C.D., and Paillet, F.L., 2011, A computer program for flow-log analysis of single holes (FLASH): Ground Water, accessed July 15, 2015, at http://dx.doi.org/10.1111/j.1745-6584.2011.00798.x.

Fairchild, G.M., Lane, J.W., Jr., Voytek, E.B., and LeBlanc, D.R., 2013, Bedrock topography of western Cape Cod, Massachusetts, based on bedrock altitudes from geologic borings and analysis of ambient seismic noise by the horizontal-to-vertical spectral-ratio method: U.S. Geological Survey Scientific Investigations Map 3233, 1 sheet, maps variously scaled, 17-p. pamphlet, on one CD–ROM.

Handman, E.H., and Bingham, J.W., 1980, Effects of selected sources of contamination on ground water quality at seven sites in Connecticut: U.S. Geological Survey Open-File Report 79–1596, 63 p.

Johnson, C.D., Dunstan, A.M., Mack, T.J., and Lane, J.W., Jr., 1998, Borehole-geophysical characterization of a fractured-bedrock aquifer, Rye, New Hampshire: U.S. Geological Survey Open-File Report 98–558, 61 p.

Johnson, C.D., and Joesten, P.K., 2005, Analysis of borehole-radar reflection data from Machiasport, Maine, December 2003: U.S. Geological Survey Scientific Investigations Report 2005–5087, 44 p.

Johnson, C.D., and Lane, J.W., Jr., 2016, Statistical comparison of methods for estimating sediment thickness from horizontal-to-vertical spectral ratio (HVSR) seismic methods—An example from Tylerville, Connecticut, USA *in* Symposium on the Application of Geophysics to Engineering and Environmental Problems, March 20–24, 2016, Denver, Colorado, Proceedings: Denver, Colo., Environmental and Engineering Geophysical Society, 7 p.

Johnson, C.D., Mondazzi, R.A., and Joesten, P.K., 2011, Borehole geophysical investigation of a formerly used defense site, Machiasport, Maine, 2003–2006: U.S. Geological Survey Scientific Investigations Report 2009–5120, 333 p., accessed May 2011 at http://pubs.usgs.gov/sir/2009/5120/.

Keys, W.S., 1990, Borehole geophysics applied to groundwater investigations: U.S. Geological Survey Techniques of Water-Resources Investigations, book 2, chap. E2, 150 p.

Lane, J.W., Jr., Haeni, F.P., and Williams, J.H., 1994, Detection of bedrock fractures and lithologic changes using borehole radar at selected sites, *in* Fifth International Conference on Ground-Penetrating Radar, Kitchner, Ontario, Canada, June 12–16, 1993, Proceedings: Kitchner, Ontario, Waterloo Center for Groundwater Research, p. 577–591.

Lane, J.W., Jr., Joesten, P.K., Pholl, Greg, and Mihevic, Todd, 2001, Analysis of borehole-radar reflection logs from selected HC boreholes at the Project Shoal Area, Churchill County, Nevada: U.S. Geological Survey Water-Resources Investigations Report 01–4014, 23 p.

Lane, J.W., Jr., White, E.A., Steele, G.V., and Cannia, J.C., 2008, Estimation of bedrock depth using the horizontal-to-vertical (H/V) ambient-noise seismic method, *in* Symposium on the Application of Geophysics to Engineering and Environmental Problems, April 6–10, 2008, Philadelphia, Pennsylvania, Proceedings: Denver, Colo., Environmental and Engineering Geophysical Society, 13 p.

Lundgren, Lawrence, 1963, The bedrock geology of Deep River quadrangle: State Geological and Natural History Survey of Connecticut Quadrangle Report 13, 40 p.

Paillet, F.L., 1998, Flow modeling and permeability estimation using borehole flow logs in heterogeneous fractured formations: Water Resources Research, v. 34, no. 5, p. 997–1010.

Paillet, F.L., 2000, A field technique for estimating aquifer parameters using flow log data: Ground Water, v. 38, no. 4, p. 510–521.

Paillet, F.L., 2004, Borehole flowmeter applications in irregular and large diameter boreholes: Journal of Applied Geophysics, v. 55, nos. 1–2, p. 39–59.

Paillet, F.L., Hess, A.E., Cheng, C.H., and Hardin, E.L., 1987, Characterization of fracture permeability with high-resolution vertical flow measurements during borehole pumping: Ground Water, v. 25, no. 1, p. 28–40.

Parker, B.L., 2007, Investigating contaminated sites on fractured rock using the DFN Approach: U.S. Environmental Protection Agency, Office of Superfund Remediation and Technology Innovation, p. 150–168, accessed August 15, 2016, at https://clu-in.org/products/siteprof/2007fracrock/028Parker,B.pdf.

Rodgers, John, 1985, Bedrock geological map of Connecticut: Connecticut Geological and Natural History Survey, Connecticut Natural Resources Atlas Series, 2 sheets, scale 1:125,000.

Shapiro, A.M., 2001, Characterizing ground-water chemistry and hydraulic properties of fractured rock aquifers using the multifunction Bedrock-Aquifer Transportable Testing Tool (BAT^3): U.S. Geological Survey Fact Sheet 075–01, 4 p.

Shapiro, A.M., and Hsieh, P.A., 1998, How good are estimates of transmissivity from slug tests in fractured rock?: Ground Water, v. 36, no. 1, p. 37–48.

Shapiro, A.M., Hsieh, P.A., and Haeni, F.P., 1999, Integrating multidisciplinary investigations in the characterization of fractured rock, *in* Morganwalp, D.W., and Buxton, H.T., eds., U.S. Geological Survey Toxic Substances Hydrology Program—Proceedings of the technical meeting, Charleston, South Carolina, March 8–12, 1999: U.S. Geological Survey Water-Resources Investigations Report 99–4018C, v. 3, p. 669–680.

Srivastav, S.K., Lubexynski, M.W., and Biyani, A.K., 2007, Upscaling of transmissivity, derived from specific capacity—A hydrogeomorphological approach applied to the Doon Valley aquifer system in India: Hydrogeology Journal, v. 15, p. 1251–1264.

Stone, J.R., Schafer, J.P., London, E.H., DiGiacomo-Cohen, M.L., Lewis, R.S., and Thompson, W.B., 2005, Quaternary geologic map of Connecticut and Long Island Sound Basin: U.S. Geological Survey Scientific Investigations Map 2784, 2 sheets, maps variously scaled, 72-p. pamphlet.

Terzaghi, R.D., 1965, Sources of error in joint surveys: Geotechnique, v. 15, p. 287–304.

Todd, D.K., 1980, Groundwater Hydrology (2d ed.): New York, Wiley, 535 p.

U.S. Geological Survey, 2015, Hebron Gneiss: U.S. Geological Survey Mineral Resources On-Line Spatial Data, accessed July 15, 2015, at http://mrdata.usgs.gov/geology/state/sgmc-unit.php?unit=CTSOh%3B0.

Williams, J.H., and Johnson, C.D., 2004, Acoustic and optical borehole-wall imaging for fractured-rock aquifer studies: Journal of Applied Geophysics, v. 55, nos. 1–2, p. 151–159.

Williams, J.H., and Paillet, F.L., 2002, Characterization of fractures and flow zones in contaminated shale at the Watervliet Arsenal, Albany County, New York: U.S. Geological Survey Open-File Report 01–385, 26 p.

Appendixes 1–7

[Appendix files are available in ZIP file format at http://dx.doi.org/10.3133/ds1020.]

Appendix 1. Borehole-Geophysical Logs From Borehole 1640–SR in the Tylerville Study Area, Haddam, Connecticut, 2014

Appendix 1 includes "Appendix1_TY-1640-SR_readme.txt," a summary of appendix contents by file and a list of abbreviations used; "Appendix1_TY-1640-SR_StdLogs.las," standard logs in Log ASCII Standard, version 2.0 (LAS2), format (details available at http://www.cwls.org/wp-content/uploads/2014/09/LAS_20_Update_Jan2014.pdf); and the following figures and tables.

Appendix 2. Borehole-Geophysical Logs From Borehole 76–BR in the Tylerville Study Area, Haddam, Connecticut, 2014

Appendix 2 includes "Appendix2_TY-76-BR_readme.txt," a summary of appendix contents by file and a list of abbreviations used; "Appendix2_TY-76-BR_StdLogs.las," standard logs in Log ASCII Standard, version 2.0 (LAS2), format (details available at http://www.cwls.org/wp-content/uploads/2014/09/LAS_20_Update_Jan2014.pdf); and the following figures and tables.

Appendix 3. Borehole-Geophysical Logs From Borehole 85–BR in the Tylerville Study Area, Haddam, Connecticut, 2014

Appendix 3 includes "Appendix3_TY-85-BR_readme.txt," a summary of appendix contents by file and a list of abbreviations used; "Appendix3_TY-85-BR_StdLogs.las," standard logs in Log ASCII Standard, version 2.0 (LAS2), format (details available at http://www.cwls.org/wp-content/uploads/2014/09/LAS_20_Update_Jan2014.pdf); and the following figures and tables.

Appendix 4. Borehole-Geophysical Logs From Borehole 79/81–BR in the Tylerville Study Area, Haddam, Connecticut, 2014

Appendix 4 includes "Appendix4_TY-79-81-BR_readme.txt," a summary of appendix contents by file and a list of abbreviations used; "Appendix4_79-81-BR_StdLogs.las," standard logs in Log ASCII Standard, version 2.0 (LAS2), format (details available at http://www.cwls.org/wp-content/uploads/2014/09/LAS_20_Update_Jan2014.pdf); and the following figures and tables.

Appendix 5. Borehole-Geophysical Logs From Borehole 77–LMR in the Tylerville Study Area, Haddam, Connecticut, 2014

Appendix 5 includes "Appendix5_TY-77-LMR_readme.txt," a summary of appendix contents by file and a list of abbreviations used; "Appendix5_TY-77-LMR_StdLogs.las," standard logs in Log ASCII Standard, version 2.0 (LAS2), format (details available at http://www.cwls.org/wp-content/uploads/2014/09/LAS_20_Update_Jan2014.pdf); and the following figures and tables.

Appendix 6. Borehole-Geophysical Logs From Borehole 130–LMR in the Tylerville Study Area, Haddam, Connecticut, 2014

Appendix 6 includes "Appendix6_TY-130-LMR_readme.txt," a summary of appendix contents by file and a list of abbreviations used; "Appendix6_TY-130-LMR_StdLogs.las," standard logs in Log ASCII Standard, version 2.0 (LAS2), format (details available at http://www.cwls.org/wp-content/uploads/2014/09/LAS_20_Update_Jan2014.pdf); and the following figures and tables.

Appendix 7. Borehole-Geophysical Logs From Borehole 95–BR in the Tylerville Study Area, Haddam, Connecticut, 2014

Appendix 7 includes "Appendix7_TY-95-BR_readme.txt," a summary of appendix contents by file and a list of abbreviations used; "Appendix7_TY-95-BR_StdLogs.las," standard logs in Log ASCII Standard, version 2.0 (LAS2), format (details available at http://www.cwls.org/wp-content/uploads/2014/09/LAS_20_Update_Jan2014.pdf); and the following figures and tables.

For more information concerning this report, contact:
Chief, Branch of Geophysics
Office of Groundwater
U.S. Geological Survey
11 Sherman Place, Unit 5015
Storrs, CT 06269
jwlane@usgs.gov
or visit our Web site at:
http://water.usgs.gov/ogw/bgas

Publishing support by:
The Pembroke Publishing Service Center

USGS

Johnson and others—**Characterization of Fractures and Flow Zones in a Contaminated Crystalline-Rock Aquifer, Tylerville, Connecticut**—Data Series 1020

ISSN 2327-638X (online)
http://dx.doi.org/10.3133/ds1020